NBSIR 78-1429 (Navy)

The Role of Passive Film Growth Kinetics and Properties in Stress Corrosion and Crevice Corrosion Susceptibility

J. Kruger, J. R. Ambrose, J. J. Carroll, and A. J. Melmed

Corrosion and Electrodeposition Section
Metallurgy Division
Institute for Materials Research
National Bureau of Standards
Washington, D.C. 20234

November 1977

Technical Summary Report No. 8

Issued May 1978

Prepared for

Office of Naval Research
Department of the Navy
Arlington, Virginia 22217

NBSIR 78-1429 (Navy)

THE ROLE OF PASSIVE FILM GROWTH KINETICS AND PROPERTIES IN STRESS CORROSION AND CREVICE CORROSION SUSCEPTIBILITY

J. Kruger, J. R. Ambrose, J. J. Carroll, and A. J. Melmed

Corrosion and Electrodeposition Section
Metallurgy Division
Institute for Materials Research
National Bureau of Standards
Washington, D.C. 20234

November 1977

DISTRIBUTION OF THIS DOCUMENT IS UNLIMITED

Issued May 1978

Prepared for
Office of Naval Research
Department of the Navy
Arlington, Virginia 22217

U.S. DEPARTMENT OF COMMERCE, Juanita M. Kreps, *Secretary*

Dr. Sidney Harman, *Under Secretary*

Jordan J. Baruch, *Assistant Secretary for Science and Technology*

NATIONAL BUREAU OF STANDARDS, Ernest Ambler, *Director*

PART I

Field Ion Microscopy Studies of the Interaction of Hydrogen with Selected Metals and Alloys

J. J. Carroll, A. J. Melmed and J. Kruger
Institute for Materials Research
National Bureau of Standards
Washington, D. C. 20234

The entry of hydrogen into a metal's lattice is known to lead to the phenomenon called hydrogen embrittlement for some alloy systems. It is not known, however, why some alloys suffer such hydrogen damage and others do not. It is not even clear which alloys do suffer such damage. For example, it is controversial as to whether the stress corrosion of austenitic stainless steel is due to hydrogen entry into the alloy's lattice or to the mechanisms not involving hydrogen. Moreover, if hydrogen damage is known to occur, its mechanism if, indeed, there is a single mechanism, is poorly understood and controversial (1).

In order to provide further insights into how hydrogen entry into a lattice produces conditions that lead to sub-critical crack growth, it would be valuable to examine on an atomic scale if possible, the rearrangements, new phase formations and other disturbances that hydrogen produces when it enters a metal lattice. The possibility for making such examinations exists through the use of field ion microscopy (FIM). Recently, this laboratory completed a study on the effects of hydrogen entry into the lattice of titanium using FIM (2). The results obtained by FIM for the beginning steps of hydrogen entry agreed with earlier eletron microscopy studies with regard to the crystallographic relationships found for titarium hydride formation. In the Ti studies the hydrogen was introduced as a gas by using it as an imaging gas. The stress required for hydrogen entry was provided by the high fields present when using FIM. Hancock and Johnson (3) have shown that in microscopic systems sub-critical crack growth can be produced in low pressure hydrogen.

The work described here seeks to extend the earlier Ti study by applying the FIM to an examination of the effect of gaseous hydrogen on a number of alloys and uranium, a metal known to suffer extensive hydrogen damage. In the group of alloys studied are 1080 steel, 304 stainless steel and Fe-24% Cr alloy.

EQUIPMENT

The field ion microscope was equipped with a 75 mm diam microchannel plate image intensifier, and a specimen-quick-change chamber for rapid specimen insertion and withdrawal. Routinely, images from two specimens could be obtained within a half an hour's time. This was an important advantage in the following studies involving the hydrogen interaction with several types of specimens, pure metals and alloys, subjected to a variety of environmental and preimaging treatments promoting hydrogen/metal interactions. Furthermore, the images obtained were generally unstable, thus requiring image intensification in order to achieve the necessarily fractional second, photographic exposure times. The specimen temperatures below room temperature were controlled by adjusting the flow of cold gaseous helium from a liquid helium dewar over specimen-mount-feed-through pin. During field ion microscopy reagent grade imaging

gases were continuously flowed through the imaging chamber. Imaging gas mixtures were made by simultaneously opening the appropriate leak valves, and mixture compositions were estimated from pressure gage measurements.

SPECIMENS

MATERIAL	SPECIMEN PREPARATION PROCEDURE
1. 12 mil diam piano wire, 1080 type, high strength carbon steel, annealed in vacuum, 800C, 24 hrs	a) reduce diam and taper, 10% $HClO_4$ in methanol, 15-5Vdc. b) polish to a sharp point, thin liquid film 1% $HClO_4$ in glycerin, 35Vdc while observing at 100X c) frequent methanol washes
2. Fe-24%Cr block from which 20 mil diam rods were spark cut	a) same as 1a except 12-2Vdc b) same as 1b except 2Vdc c) frequent methanol washes
3. 304 stainless steel, 5 mil diam wire	a) reduce diam and polish to a sharp point in 10% $HClO_4$ in methanol, 50Vdc OR sharpen tip in 10% HCl, aqueous thin liquid film while observing at 100X b) water or methanol rinse
4. iron whiskers blade shape	a) use thin liquid film of 1:1:2 HCl, HNO_3, H_2O, 2-3Vdc OR 10% HCL, aqueous, 1-2Vac, and observe at 100X b) frequent water washes
5. depleted uranium, 20 mil diam wire, ortho-rhombic phase, annealed 5 days 620C	a) reduce diam and taper using 4 gm citric acid, 1 ml HNO_3, 200 ml H_2O, 40-20Vac b) use thin liquid film of same solution to sharpen, 20-25Vac, while observing at 100X c) frequent methanol washes

1080 HIGH STRENGTH CARBON STEEL

Field ion micrographs obtained from this material showed a high degree of order among the imaging spots indicating cubic symmetry. Fig. 1 shows a field ion micrograph of 1080 steel imaged with a helium-neon gas mixture. Boundaries (arrows) appeared often in field ion micrographs obtained from this material. Pending further analysis the boundaries may correspond either to low angle grain boundaries or twin boundaries, but, for the present, the boundaries are referred to as grain boundaries. The metal's surface did not appear to be obscurred by the presence of a surface film. Generally, disordered alloys and adsorbed metal films tend to image as a random array of spots. More importantly, interpretation of field ion microscopy studies of the material's interaction with hydrogen may proceed straightforwardly without the necessity of considering the influence of an intervening adsorbed layer.

Exposing 1080 steel to hydrogen gas, with or without the presence of the electric field, at a specimen temperature of about 30K, did not have any apparent effect on the steel. Fig. 2 shows a hydrogen field ion micrograph (no helium or neon present) of the same specimen used in Fig. 1. More surface atoms were imaged using hydrogen than using helium-neon gas mixtures. The apparent gap between grains was lessened as more atoms appeared closer to the boundary edge. The crystal planes intersected by the grain boundary retained their definition and integrity, indicating no adverse interaction in those areas, at least. Fig. 3 shows another helium-neon field ion micrograph (without hydrogen) of the same specimen immediately after it was subjected to the above described hydrogen treatment. No adverse effects are apparent. Fig. 3 appears more regular than Fig. 1 because the imaged area was enlarged by field evaporation during the hydrogen experiment thereby exposing more step edges to the imaging electric field.

Exposing titanium and zirconium to similar hydrogen treatments in the field ion microscope caused micro-cracks and fissures to form in both metals, and caused crystal planes to appear ruptured (2,4). These effects were crystallographically specific in each case, and titanium appeared to be more sensitive to hydrogen than zirconium (4). Clearly, in the present case of 1080 steel, this did not occur.

A more severe interaction of 1080 steel with hydrogen was observed at room temperature. Although field ion micrographs show less than optimum resolution when the specimen is at room temperature, one can see in Fig. 4 a generally gray field corresponding to an adsorbed film, and a darker central area where the previously adsorbed film was removed by the applied electric field exposing the 1080 steel substrate. The exposed steel was rapidly field evaporating under these imaging conditions. As a result, only a couple of net plane rings were photographed but many more were observed. On the other hand, the adsorbed film appeared stable at best imaging conditions, with the exception of the interesting bright streaks seen concentrated in the upper part of Fig. 4. The streaks were unstable in that they appeared to move about the film surface, and to change in length. The relatively large ion currents giving rise to the bright lines may be due to ridge formation on the adsorbed film brought about by the imaging process. Similarly unstable, bright spotted lines were observed at cracks formed in titanium observed with hydrogen field ion microscopy at 25K (2). With correspondingly low temperature imaging applied to the present case, it may be possible to improve resolution of the room temperature formed film and streaks in order to increase our present understanding of this interesting feature.

Further film desorption proceeded by exposing the specimen momentarily to higher applied voltages than best image voltage. However, in the wake of the receding film, patches of newly formed film adsorb on the freshly exposed field evaporating steel substrate. Fig. 5 shows a micrograph of the same specimen following further film desorption. The crescent shaped area at the far left shows the remaining adsorbed film of Fig. 4. The newly adsorbed film patches are brighter than the primary adsorbed film (crescent area), and are unstable in that the film patches appear and disappear with time. The dim spotted background image is due to the 1080

steel substrate, rapidly field evaporating under imaging conditions. Fig. 6 shows improved resolution of the same film and substrate as shown in Fig. 5, brought about by cooling the specimen with liquid nitrogen coolant.

The general location of the bright streaks on the room temperature film shown in Fig. 4 corresponds in part, but not completely, to the adsorption sites of film patches shown in Fig. 5. It is not known, at present, whether the film patches of Fig. 5 have the same chemical composition and structure as the adsorbed film of Fig. 4. The damage, if any, incurred by the 1080 steel substrate as a result of exposure to hydrogen at room temperature has not been determined.

Additional experiments were attempted in which 1080 steel specimens, following tip sharpening procedures, were cathodically polarized between 5 and 10 volts in an aqueous 10% $HClO_4$ solution for a few seconds in order to increase the amount of hydrogen incorporated into the metal lattice. Cathodic charging adversely affected a specimen's lifetime, that is all specimens prematurely failed during field ion microscopy. No specimen survived neon field ion evaporation and imaging conditions long enough to obtain a crystallographic map of the steel substrate. However, room temperature hydrogen imaging produced similar films as those in Figs. 4 - 6. Further studies are necessary to establish the effect that hydrogen may have on 1080 steel lattice and grain boundaries that are visible with field ion microscopy.

304 STAINLESS STEEL

Generally, 304 stainless steel did not image as well as 1080 steel in that most spots in the field ion micrographs appeared to be randomly distributed. From the few net plane rings that did appear about the surface, there was not enough information to crystallographically index micrographs. For example, some net plane rings appeared in the central grain of Fig. 7 (arrows). The central grain was roughly elliptical in cross section and distinguished from the other grain by a dark, finite width line. During the course of field evaporation the central grain became smaller in size and finally disappeared. In summary, there is a modicum of ordered spots in a typical field ion micrograph of stainless steel, and evidence that grain boundaries are visible.

Stainless steel/hydrogen interaction experiments were carried out at 30K. No changes were detected in the appearance of the pertinent field ion micrographs. The reason for this may be due to the presence of an adsorbed, contamination layer (giving rise to micrographs showing little overall crystallographic order) interfering or altering the hydrogen/stainless steel interaction that would occur otherwise.

IRON - 24% CHROMIUM

Fig. 8 shows a neon field ion micrograph obtained from an Fe-24% Cr specimen. Field ion micrographs obtained from Fe - 24% Cr and 304 stainless steel (Figs. 7 and 8) show similar imaging characteristics, - only a few net crystal plane rings visible in a field of disordered spots. Exposing and imaging with hydrogen gas produced completely disordered field ion micrographs (Fig. 9) indicating that these imaging conditions may have produced an adsorbed film.

Evidence was obtained that suggests that the images of Figs. 8 and 9 came from an adsorbed film, at least in part. Fig. 10 is a field ion micrograph obtained from the same specimen that was used in Figs. 8 and 9, but imaged in a peculiar way that deviates from usual field ion microscopy practice. The specimen was subjected to a several thousand volt pulse over the voltage required for imaging. During the pulse the specimen surface was dramatically destabilized and several hundred layers were removed quickly by the field evaporation process. Stabilizing the image again at best image voltage, Fig. 10 was obtained. The pattern is regular enough to be crystallographically indexed. The specimen may be clean enough to permit examination of its hydrogen interaction in more detail. Furthermore, the pulse field evaporation technique applied to 304 stainless steel may produce improved field ion micrographs.

IRON

It is known (5) that pure iron field ion micrographs show excellent overall order and atomic detail on the (110), (100), (112) and higher order crystal planes, and with special care taken to exclude minute quantities of hydrogen in the gas phase, the (111) crystal plane as well. With normal background partial pressures of hydrogen in unbaked, ion pumped, metal vacuum systems, the (111) plane area images do not show net plane rings among the imaging spots (5). See Fig. 11. The (111) plane area of iron appears to be more sensitive to hydrogen than other crystal planes. Hydrogen field ion micrographs of iron obtained at 30K, as shown in Fig. 12, retained net (110) and (100) crystal plane order but the (111) plane area became move disordered and imaged more brightly. However, hydrogen imaging conditions at 30K did not have any lasting effect on iron, for when neon was substituted for hydrogen as the imaging gas, the (111) plane areas imaged first and quickly ordered during field evaporation as the rest of the crystal areas imaged in ordered fashion. No evidence in the iron field ion micrographs was found that indicated defective or irregularly shaped crystal planes, micro-crack defects of adsorbed films.

Severe corrosion of iron occurred, however, when iron was exposed to trace amounts of air during neon field ion microscopy. Fig. 13 shows an iron field ion micrograph obtained under these conditions. No spots were observed in the (111) plane area, indicating that a hole or pit was formed in this area, perhaps, as a result of preferential field evaporation of reaction products at significantly less field strengths than that required for neon imaging.

URANIUM

Figure 14 shows a field ion micrograph obtained from uranium. Until now, no orthorhombically structured element has been successfully imaged in the field ion microscope. The image in Fig. 14 was obtained from a single crystalline grain. The image contains many crystal planes continuously distributed about adjoining and symmetrically disposed bright and dark contrast field regions. The problem of crystallographically indexing uranium field ion micrographs has not been resolved. Presently, the grain size of the source material is too small to obtain single crystalline x-ray diffraction patterns.

After prolonged imaging using hydrogen, patterns typified by Fig. 15 were obtained. The pattern shows several grain boundaries and irregularly shaped grains ranging between about 5-30 nm in breadth. After replacing hydrogen imaging gas with neon, followed by considerable field evaporation, it was found that the small grained surface image was followed by a uniformly disordered image that, upon further field evaporation, showed film desorption characteristics. As the disordered film desorbed an image with similar characteristics as Fig. 14 was exposed. The evidence indicates that the micrograph in Fig. 15 was obtained from a surface hydride of uranium. Supporting evidence was found by exposing a uranium specimen, showing neon images similar to Fig. 14, to hydrogen field ion imaging conditions. A disordered film formed immediately, followed by the gradual formation of randomly scattered small clusters of bright spots, the number and size of the clusters increasing with hydrogen exposure time. Figs. 16 (a,b) were obtained during this experiment after about 15 and 30 minutes of hydrogen field ion microscopy, respectively. These field ion microscopy experiments indicate that, in the case of uranium in the presence of hydrogen field ion imaging conditions, an adsorbed layer was formed followed by nucleation and growth of uranium hydride.

CONCLUSIONS

In the foregoing studies an attempt was made to broaden our current knowledge of the interaction of hydrogen with pure metals and alloy steels by using the technique of field ion microscopy. Through the application of this technique many microscopic details were observed under the experimental conditions imposed by the technique, namely hydrogen adsorption on field evaporated surfaces in the presence of large electric fields. The following list includes the presently obtained results. It is apparent however, that further work is necessary in order to complete the investigations.

1. No evidence was found that indicated that 1080 steel was effected adversely by its interaction with hydrogen between 30-80K.

2. Although further experimentaion is necessary before the situation at room temperature is clarified regarding possible 1080 steel substrate damage brought about by its interaction with hydrogen, it was evident that substantial film adsorption occurred on specimens with or without a previous history of cathodic charging.

3. Control experiments with pure iron indicated that a) the (111) plane area was most sensitive to hydrogen, as evidenced by a damaged surface layer, and 2) the (110) and (100) planes appeared uneffected.

4. Experiments with 304 stainless steel and iron-24% chromium steel indicate that ordinary imaging techniques may not reveal film-free, clean metal surfaces. No significant effects were observed using such surfaces in hydrogen experiments. A new technique was devised that indicated

that iron-24% chromium can be cleaned from the strongly adsorbing film ordinarily observed. Further work using the revised technique is necessary in order to determine the technique's usefulness in obtaining cleaner stainless steel surfaces. Hydrogen experiments involving cleaner surfaces of iron-24% chromium and 304 stainless steel may show interesting effects that may reveal the type of interaction involved, kinetic information, and the role of alloying additives.

5. Hydrogen experiments with uranium indicate that hydrides readily form by a process of nucleation and growth on a previously formed adsorbed layer.

REFERENCES

1. R.W. Staehle, "The Theory of Stress Corrosion Cracking in Alloys" NATO Scientific Affairs Dir., Brussels, 1971 pp 231 - 243.

2. J.J. Carroll, J. Smit and A.J. Melmed, "Fielding-ion imaging of titanium and effects due to hydrogen," Surface Sci. 45 (1974) 640 - 648.

3. G.G. Hancock and H.H. Johnson, "Hydrogen, oxygen, and subcritical crack growth in a high-strength steel," Trans Met. Soc. AIME 236 (1966) 513 - 516.

4. J.J. Carroll and A.J. Melmed, "Field ion microscopy of zirconium," Surface Sci. 58 (1976) 601 - 604.

5. Erwin W. Muller and Tien Tzou Tsong, Field Ion Microscopy; Principles and Applications (Elsevier, New York, 1969), pp. 116, 161 and 174.

Fig. 1. A field ion micrograph obtained from a 1080 steel specimen, imaged in a gas mixture of 55% helium and 45% neon, at a specimen temperature of 25K, 3750 volts.

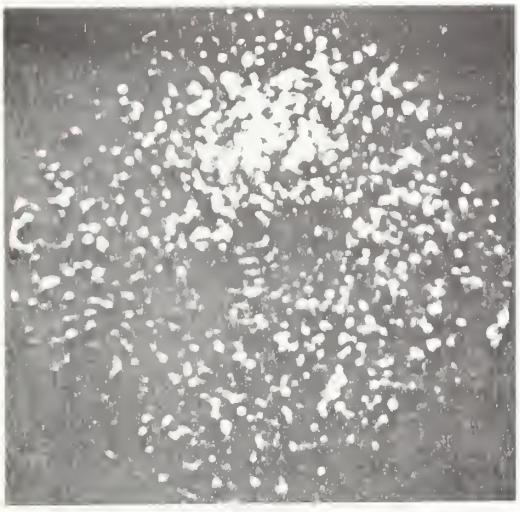

Fig. 2. A hydrogen field ion micrograph obtained from the same 1080 steel specimen as imaged in Fig. 1, 25K, 2600 volts. Note the appearance of two dark areas near the center of the micrograph. Both are artifacts that appear in most of the following micrographs.

Fig. 3. A field ion micrograph obtained from the same 1080 steel specimen as imaged in Fig. 1, following its exposure to the hydrogen imaging conditions described in Fig. 2, and imaged in a 55% helium and 45% neon gas mixture, 25K, 5000 volts.

Fig. 4. A hydrogen field ion micrograph obtained from a 1080 steel specimen at room temperature, 8800 volts. See text for additional details.

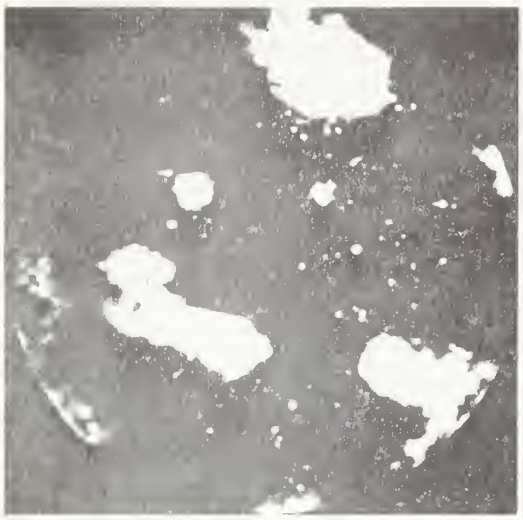

Fig. 5. A hydrogen field ion micrograph obtained from a 1080 steel specimen at room temperature, 8200 volts.

Fig. 6. A hydrogen field ion micrograph obtained from the same specimen as imaged in Fig. 5, but cooled with liquid nitrogen, 11,000 volts.

Fig. 7. A neon field ion micrograph obtained from a 304 stainless steel specimen, 30K, 12,500 volts. Arrows indicate crystal net plane rings.

Fig. 8. A neon field ion micrograph obtained from a specimen of iron - 24% chromium, cooled at 30K, 14,000 volts.

Fig. 9. A hydrogen field ion micrograph obtained from the same specimen as imaged in Fig. 8, 30K, 10,000 volts.

Fig. 10. A field ion micrograph obtained from the same specimen as imaged in Fig. 8, imaged in a neon and hydrogen gas mixture, 30K, 15,000 volts.

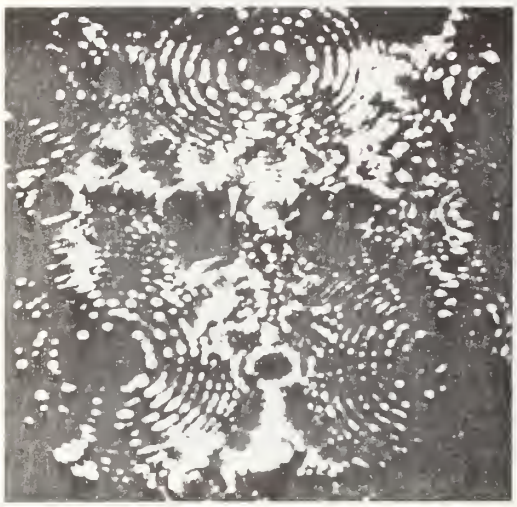

Fig. 11. A neon field ion micrograph obtained from iron, 30K, 8600 volts.

Fig. 12. A hydrogen field ion micrograph obtained from the same iron specimen as used in Fig. 11, 30K, 6600 volts.

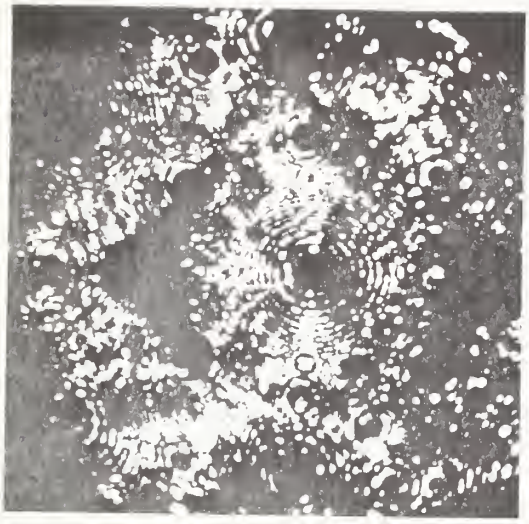

Fig. 13. A neon field ion micrograph obtained from an iron specimen exposed to a small partial pressure of air, 30K, 9400 volts.

Fig. 14. A neon field ion micrograph obtained from uranium, 30K, 15,500 volts.

Fig. 15. A hydrogen field ion micrograph obtained from uranium, 30K, 8600 volts.

16(a)
30K
14,700 volts

16(b)
30K
16,200 volts

Fig. 16 (a, b) Hydrogen field ion micrographs obtained from a uranium specimen exposed to hydrogen imaging conditions for about 15 and 30 minutes, respectively.

PART II To be published in Proceedings of 4th
International Symposium on Passivity

The Role of Noncrystalline Films in Passivation and Breakdown of Passivation

A. G. Revesz
COMSAT Laboratories
Clarksburg, MD 20734

and

J. Kruger
National Bureau of Standards
Institute for Materials Research
Washington, D.C. 20234

1. INTRODUCTION

In his 1969 Palladium Medal address, Hoar[1] set forth some "rules" to serve as guidelines for producing alloys that would exhibit the best corrosion resistance because of their ability to form superior passive films. One guideline of his is to use metals in an alloy that lead to the formation of "mixed" oxides involving polyanions which result in "cross-linked monolithic amorphous structures not containing the extremely defective grain boundary regions of polycrystalline materials". Due to the lack of grain boundaries in such a noncrystalline film, the outward migration of cations is reduced.

Subsequent to this suggestion by Hoar, there were a number of experiments and discussions that have served to bolster his insight. For example, McBee and Kruger[2] showed by electron diffraction that as one adds Cr to Fe in an alloy the films formed go from polycrystalline to noncrystalline structure with increasing Cr content. According to Okamoto[3] "the most important parameter controlling the corrosion resistance of [stainless] steel is concluded to be the amorphous nature of the film in which bound water is included." Leach[4] has also noted that glassy films tend to promote corrosion protection in many cases. He also pointed out that this enhanced corrosion resistance correlates with the greater ductility of the oxide film. Fehlner and Mott,[5] while not being concerned about passivity, asserted in a review on low-temperature oxidation that "an oxide film formed at low temperature is amorphous." They have suggested that, depending on whether the oxide is a "network former" or "network modifier" (using Zachariasen's[6] criteria)*, the amorphous film is with or without a network structure, and that this structural difference determines the transport process. However, details of the noncrystalline structure, particularly in the case of network modifiers, were not discussed. Lawless[7] has pointed out in his review that the low temperature oxide films on Cu, Ni, Zn, and Fe are known to be crystalline. Some aspects of Fehlner and Mott's assertion concerning the formation of amorphous oxide film on aluminum have been critized by Pryor.[8]

---

*An important feature of the glass network is that oxygen atoms (ions) form M-O-M bridges, i.e., their coordination is two.

Judging from the examples just described and others, it appears that there is increasing evidence that an important aspect of the beneficial properties of some passive films are in many instances related to their noncrystalline structure. From the viewpoint of passivation, very little attention has thus far been given to a detailed examination of what are the structural characteristics of noncrystalline oxide films on metals. Are there different types of noncrystallinity? What factors influence the structure and stability of noncrystalline films; what effect do these factors have on passivity and on breakdown of passivity?

These questions are also very pertinent to some other areas outside passivation. Closely related to passivation is the formation and properties of anodic oxide films, many of which are noncrystalline (e.g. Ta_2O_5, Al_2O_5).[9] The importance of non-crystallinity for oxides used as dielectric films in capacitors has been pointed out by Harrop and Campbell[10] but without discussing the fundamental problems of structure.

Some fundamental questions have been discussed from 1967 on in connection with SiO_2 films on silicon.[11] This film is used to stabilize the surface properties of silicon devices; the discovery in 1959 by Atalla et al.,[12] that thermal oxidation of silicon stabilizes, i.e. passivates, its surface, was a crucial step in semiconductor device technology. Revesz[13] has reviewed the surface passivation of silicon emphasizing the importance of noncrystallinity.* More recently, the work has been extended to noncrystalline Ta_2O_5 films on silicon. [14],[15]In the course of these studies, concepts and results developed that appear to be pertinent to understanding the role of noncrystallinity in influencing the properties of passive films on metals.

From the classic point of view of passivity, films on silicon may not seem relevant. However, since the Si/SiO_2 interface is the best understood solid/solid interface and SiO_2 is a non-crystalline (vitreous) solid par excellence, the passivation and oxidation behavior of silicon can be used as a basis of comparison in discussing more conventional systems such as stainless steel. It is, thus, the plan of this paper to develop a comprehensive discussion of noncrystallinity using the oxide films of Si and Ta as a basis and then to discuss the role that noncrystallinity can play in passivity and the breakdown in passivity in general.

---

*The development of integrated circuits and, thus, today's computer industry is largely due to the excellent properties of vitreous SiO_2 film and its interface with the Si substrate. This has been a very sophisticated applications of semiconductor surface passivation which is very close indeed to passivation of metals.

2. NONCRYSTALLINE OXIDE FILMS AND FILM/SUBSTRATE INTERFACES

In this section, various aspects of noncrystalline oxide films and film/substrate interfaces will be discussed using SiO_2 and Ta_2O_5 films as examples. These two oxide films are used to demonstrate the importance of bond and structural flexibility in noncrystalline structures. The usefulness of these concepts will be illustrated on a few other oxides which are important from the viewpoint of metal passivation.

2.1 The Si/SiO_2 Interface Structure

Silicon single crystal is the most perfect and best understood solid. Owing to its great importance in semiconductor device technology, the Si/SiO_2 interface has been extensively studied. An important factor in these investigations has been that the noncrystalline SiO_2 films are prepared on a very perfect substrate under very clean conditions. As a result, the SiO_2 films are also quite perfect. The electronic properties of the Si substrate are very sensitive indicators of the perfection of the SiO_2 film, including the Si/SiO_2 interface, unsurpassed by any other physicalchemical analytical technique. This is why the Si/SiO_2 interface has emerged as the best characterized solid/solid interface. This section is essentially based on a review,[13] and works listed in the bibliography there are not referenced here.

Silicon is a very electropositive element but, in practice, it is inert in aqueous media due to the passivating oxide film. This noncrystalline oxide film forms at a logarithmic rate in room temperature conditions reaching a thickness of about 3-4Å.[16] This behavior is similar, among others, to that of aluminum or tantalum; but, in contrast to these metals, thermal oxidation of silicon (even at very high temperatures) results in a noncrystalline SiO_2 film. The perfection of thermally grown SiO_2 films can be illustrated by the low density of sodium impurity ($<10^{15}$ cm^{-3}) and electron trapping defects ($<10^{14}$ cm^{-3}), high dielectric breakdown strength ($>10^6$ V cm^{-1}), excellent reproducibility, and stability under extreme conditions.

The perfection of the Si/SiO_2 interface is demonstrated by the very low density of interface states: $<\sim 10^{10}$ cm^{-2} (corresponding to $\sim 10^{-5}$ monolayer adsorbate). These interface states are associated with unsaturated ("dangling") bonds of surface Si atoms (which at an ideal Si/SiO_2 interface should be bonded to oxygen atoms) and/or with electron (hole) trapping defects in the oxide film within tunneling distance ($<\sim$15Å) from the interface. These interface states may act as localized traps for electronic (holes) in the silicon and, thus, adversely affect its electronic properties. Also, they represent chemically active sites and, as such, they were responsible for the surface instability effects which plagued semiconductor devices before the discovery of surface passivation. In

this latter sense, interface states at the Si/SiO_2 interface are, to some extent, similar to active sites in metal/passivating film interface structures which play such an important role in the breakdown of passivation.

The high perfection of the SiO_2 film and of the Si/SiO_2 interface is due to the noncrystalline structure of SiO_2. When the film begins to crystallize (e.g., during prolonged heat treatment at high temperature) the properties of the film (e.g. dielectric strength) deteriorate and the density of interface states increases. The first effect results from the disruption of the Si-O network as crystallites form. This process is associated with the generation of network defects and, later, even with the formation of grain boundaries between crystallites. As was already mentioned in the Introduction, the presence of grain boundaries in the oxide film leads to the loss of its passivating (protective) character. Thus, a polycrystalline or highly defective noncrystalline oxide film is not a good candidate for passivation.

The increase in interface state density during crystallization of the SiO_2 film results from the loss of structural flexibility characteristic of the SiO_2 film while it is noncrystalline. As a result of this flexibility, the majority of the surface Si atoms can be bonded to an oxygen atom of the oxide without requiring an almost perfect epitaxial relationship between Si and SiO_2. When, however, the SiO_2 film is crystalline, the match of two structures with rigidly defined but different long-range order is poor and, hence, the interface is disordered. Apparently, quasi-perfect solid/solid interfaces can be only obtained when either a quasi-perfect epitaxial relationship exists between two single crystals or at least one side of the interface is noncrystalline. This conclusion is obviously very pertinent to the passivation of metals which are usually (but not exclusively) polycrystalline and, therefore, an epitaxial relationship with the oxide film is out of the question. Thus, elimination or drastic reduction of the active sites in the thin passive film requires that the passivating film be noncrystalline.

It can be seen from the above discussion that SiO_2 films can be very perfect in spite of, rather, because of the fact that they are noncrystalline. The reason for this is that the lack of long-range order does not simply arise from a destruction of structural order altogether. Rather, the short-range-order characteristic of crystalline polymorphs of SiO_2 is maintained in noncrystalline SiO_2 films, as well as in fused silica; that is, every Si atom is surrounded tetrahedrally by four O atoms and the Si-O bond length is constant. It is the Si-O-Si bridging bond angle which is characterized by a wide distribution (from $\sim$120° to 180°) in vitreous SiO_2. Because of this distribution it is possible to establish a Si-O network without long range order and without breaking many Si-O bonds and, hence, introducing a large number of defects. This type of noncrystalline structure has been named

vitreous in contrast to amorphous noncrystalline structures which do not have appreciable short-range order.[11] Fused silica and SiO_2 films on silicon are vitreous solids par excellence, whereas, for instance, vacuum deposited SiO is an amorphous solid. The lack of short-range order in amorphous solids is usually associated with chemical disorder, whereas the short-range order in vitreous solids ensures perfect stoichiometry and excellent reproducibility.

The structural flexibility of SiO_2 is also manifested in the large number (9) of crystalline polymorphs which have essentially identical short-range order and almost the same standard free enthalpy of formation (the difference between quartz and fused SiO_2 is about 1 percent); yet, they exhibit significant variations in several properties, e.g., density, bond polarizability, etc.* The reason for this behavior is that various topological arrangements of $SiO_4/_2$ tetrahedra of essentially the same energy can be present in these polymorphs. Thus, similar to polymers, the variation in structure is essentially a conformational problem.

2.2 Bond Flexibility and Noncrystalline (Vitreous) Structure

The structural flexibility of SiO_2 polymorphs, including vitreous SiO_2 is due to the flexibility of the Si-O bond. This bond is partially ionic (~40%) and partially covalent (~60%) and the covalent part has σ and π components.** Apparently, the individual contributions of these components can vary without significantly affecting the total bond energy but influencing other properties. On this basis, we can visualize vitreous SiO_2 as a network built up from $SiO_4/_2$ units where a large number of local conformations of almost the same energy exist and, accordingly, the Si-O-Si angle varies greatly. *The flexibility of the Si-O bond is thus the principal reason that SiO_2 can be prepared in the vitreous state.*

The importance of partially ionic and partially covalent bonds in vitreous structures has been discussed in great detail by Myuller[17]. However, the question of bond flexibility is more complicated than the considerations of the mixed ionic-covalent bond indicate. This point is illustrated by a comparison between SiO_2 and GeO_2.

---

*With the exception of aluminum, no metal has a comparable number of oxide polymorphs. Aluminum oxide (corundum) has five polymorphs whose standard free enthalpies of formation are within 2.5% of each other.

**The σ-bond arises from sharing one of the $3sp^3$ electrons of silicon with on of the 2p valence electrons of oxygen; the π-bond is due to the overlap between the 3d orbitals of Si (empty in the ground state) and the 2p orbital of O containing the lone pair electrons.

In spite of the close resemblance of germanium to silicon, the properties of GeO_2 are rather different from those of SiO_2, even though the Ge-O bond is also a mixed ionic covalent bond, roughly in the same proportion as the Si-O bond. However, there is no π-bonding in GeO_2 because of much less overlap between the oxygen 2p and germanium 4d orbitals relative to the Si 3d orbitals. As a result, the bond flexibility is greatly reduced. Thus, there is only one GeO_2 crystalline polymorph with 4:2 coordination (hexagonal, silica structure) and the tendency toward noncrystallinity is much less than in the case of SiO_2. The lack of π-bonding in GeO_2 is also partially responsible for the significant solubility of hexagonal and noncrystalline GeO_2 in water. Hence, the thin GeO_2 film formed at room temperature does not passivate to such an extent as the SiO_2 film does, and thermally grown GeO_2 film is useless for surface passivation since it is soluble in water and chemically very reactive. This difference in the passivation behavior is the main reason that silicon has replaced germanium in semiconductor device technology.

A different kind of bond flexibility is exhibited by metals which can be in various oxidation states. Thus, for example the standard free enthalpies per g-atom of Cr are -141 and -136 kcal mole^{-1} for CrO_3 and Cr_2O_3, respectively. This difference is relatively small so that various structural conformations of roughly the same energy may exist. This could be a factor in the formation of relatively stable noncrystalline In addition, transition metal oxides, e.g. Cr_2O_3, may exhibit a departure from the regular structure due to ligand effects.[18] Since both σ- and πbonding can be involved in these effects and π-bonding can affect the stereochemistry while its contribution to the bond energy is relatively small, a situation somewhat similar to that characteristic of the Si-O bond may arise.* Even without involving π-bonding, ligand effects may increase the bond flexibility. It is possible that these effects are partially responsible for the important role of H_2O in passivation since H_2O is a σ donor ligand. The effects of H_2O will be discussed below, but it is significant to mention in this context that due to the large number of delectrons, chromium (electron configuration in ground state : $3d^5 4s^1$) can be associated with water as a ligand in several configurations; this might be an additional important factor in increasing the stability of the noncrystalline passivating film on Cr metal and in the beneficial effects of Cr alloying on corrosion.

2.3 Vitreous Ta_2O_5 Films and Structural Flexibility

It is well known that anodic oxidation of tantalum results in a noncrystalline Ta_2O_5 film whose dielectric and optical properties as well as its excellent reproducibility, indicate that there is a

---

*The O^{2-}-ion as a ligand can act as σ or π donor. In the Si-O bond the role of oxygen can be considered as similar to that of π donor ligand.

high degree of short-range order in the structure, i.e., the film is vitreous.[9] On the other hand, thermal oxidation of tantalum, both in polycrystalline and single crystalline form, usually results in polycrystalline oxides with poorly defined properties.[8,19] Apparently, the thin noncrystalline passivating film present on the Ta surface breaks down during thermal oxidation, whereas it grows further during anodic oxidation. Revesz and coworkers[14] have found that vitreous Ta_2O_5 film can also be obtained by thermal oxidation of Ta film vacuum deposited on silicon. This Ta_2O_5 film is morphologically and optically so perfect that it is used as an antireflection film in silicon solar cells of improved conversion efficiency. This vitreous Ta_2O_5 film on silicon can withstand prolonged heat treatments without crystallization. Polycrystalline Ta foil oxidized under identical conditions resulted in polycrystalline Ta_2O_5 film of very poor optical properties. These observations demonstrate that the substrate plays a great role in determining the formation and stability of a noncrystalline (vitreous) solid. This aspect will be discussed below, but the fundamental question is: why can Ta_2O_5 be obtained under some circumstances in the vitreous state?

In order to answer this question, we have to consider the structure of crystalline Ta_2O_5. According to Stephenson and Roth,[20] the structure of Ta_2O_5 is based on chains of distorted octahedral and pentagonal bipyramidal oxygen polyhedra around the Ta atoms. The coordination of oxygen in these configurations is not two; hence, simple Ta-O-Ta bridges (analog to Si-O-Si bridges) do not exist. Consequently, the Zachariasen rules of glass formation[6] are not fulfilled and, in this sense Ta_2O_5 cannot be considered as a "network former". However, it is network former on the basis of metal-oxygen bond strength.[5]

Since the Ta-O bond is ∿60 percent ionic and ∿40 percent covalent, the bond is expected to have some flexibility, even though, as was shown for the Ge-O bond, this kind of flexibility is not necessarily sufficient. Additional bond flexibility may arise from ligand field effects characteristic of transition-metal oxides as mentioned above. This is probably the reason for the large variation (from 1.83Å to 2.60Å) of the Ta-O bond length in crystalline L-Ta_2O_5 (the low temperature polymorph).[20] The structural complexity of this structure is manifested in the very large unit cell that is divided in subcells.[21] The arrangement of these subcells and the size of the unit cell depend on heat treatment and impurities such as hydrogen, silicon, etc.; for example, the unit cell formula at temperatures below 1000°C is $Ta_{28}O_{70}$.

The structural complexity is closely associated with the possibility of varying the composition (stoichiometry) by changing the relative numbers of structural subunits which are structurally closely related but differ slightly in their composition; these structures have been named "infinitely adaptive"[22] or "vernier"[23] structures. Since the difference in lattice

energy between the alternative structures arrangements is very low, the various substructures can easily interchange. In this regard, the structure of L-Ta_2O_5 exhibits a similarity to polymers and, analogously, the various arrangements of substructures might be considered as structural conformations.

It is very likely that the adaptive nature of the L-Ta_2O_5 structure plays an important role in the formation of noncrystalline Ta_2O_5. Specifically, we suggest that the increased tendency toward long-range order usually exhibited by structures in which the nonmetallic element has a coordination larger than two is counteracted to some extent by the structural complexity in Ta_2O_5. As a result, arranging the atoms according to the long-range order of the crystal during the formation of the oxide may be more difficult kinetically than forming a vitreous structure.

Since an interaction with the Si substrate occurs during the oxidation of Ta film on silicon,[15] it is interesting to note that incorporation of silicon leads to increased complexity in the unit cell of L-Ta_2O_5.[21] As a result of this increased complexity, silicon hinders the formation of the crystalline structure. Consequently, silicon facilitates the formation of a noncrystalline structure and may also stabilize it.

Since the coordination of Al and O atoms in Al_2O_3 is 6:3, the oxygen does not form Al-O-Al bridges and so this oxide also cannot strictly be considered as a network former. However, it was mentioned above that there are five polymorphs of Al_2O_3 of not too different formation energies. The structural difference among these polymorphs arises from different degrees of ordering Al atoms in an essentially closest packing of O ions.[24] This structural flexibility is quite different from that exhibited by SiO_2 but it could be important in the formation of noncrystalline Al_2O_3 as well as in other ionic oxide structures based on nearly closest packing of O ions. Such an oxide is, for instance, the Fe-Cr perovskite, which is the structure of oxide films on stainless steel with low Cr-content.[2] It is very likely that the structural flexibility of the perovskite structure increased by the incorporation of chromium and this could be the reason that at higher Cr content the passivating film is noncrystalline.

Therefore it is evident that the most important factor determining whether an oxide film can be obtained in a reasonably stable vitreous form (i.e., in a noncrystalline structure with a high degree of short-range order) so that it can passivate the underlying metal is that it must have some flexibility. This flexible structure then allows the formation of localized structural conformations having nearly the same energy. These structural units are essentially identical to those present in the crystal but they are linked together without long range order. This flexibility is more decisive than the geometric requirements. Clearly, classification of oxides into network formers and network modifiers is not sufficient. The problem of noncrystalline (vitreous) structure is

fundamentally associated with the bond/structure flexibility but many factors influencing the kinetics of formation and stability are involved. Essentially, the problem lies in kinetics rather than theromodynamics.

3. GENERAL CONSIDERATIONS OF FACTORS INFLUENCING NONCRYSTALLINE STRUCTURE

It is evident from the preceding discussion that a passivating film should be noncrystalline, preferably, vitreous in the sense of having appreciable short-range order. The intrinsic structural flexibility is obviously an important requirement but this can be modified for instance, by incorporating other atoms in the oxide film, as well as by various factors which influence the kinetics of the formation, self-repair of localized break-down, and formation of passivating noncrystalline films. Some of these factors have already been briefly mentioned in connection with the oxide films discussed above and are systematically discussed in this section.

3.1 Effects of Additives to the Oxide Film

Concerning the corrosion resistance of alloys, Hoar[1] has concluded that "we may expect mixed or compound oxides on alloys usually to be more protective than on pure metals because they will tend to be less soluble and less 'crystalline'". Additives to the oxide film can be introduced not only by alloying the metal but by surface treatments e.g., ion implantation, as reviewed recently by Ashworth et al.[25] In view of the discussion in the preceding section, it is obviously desirable that the additive enhances noncrystallinity of the passivating film. This can be achieved by increasing the structural/bond flexibility as for instance, Cr does in the passivating film on stainless steel. Another possibility is to increase the stability of the noncrystalline structure by decreasing the ease of the crystallization; incorporation of Si into Ta_2O_5, mentioned above, is an example.

Special attention should be given to hydrogen as an "additive" in oxide films. Hydrogen in the oxide film can lead to increased structural flexibility by forming M-OH bonds in addition to M-O bonds. If the corresponding metal hydroxide has various polymorphs as, for instance, AlO.OH,[26] then various conformations of the M-OH bond may exist in the H- containing passivating film; this results in increased tendency toward noncrystallinity. The M-OH groups can be linked together via hydrogen bonds as in the case of AlO-OH and CrO.OH;[26] this facilitates the formation of a noncrystalline network (cf.H-bonding in organic polymers). However, H or OH may also weaken the oxide structure in some cases. The fact, that hydroxide ions of some metals (e.g. Cr, Al, Ta, Si) can form hydrogen-bonded polymer (but not Fe, Ni, Cu, etc.)[27] is probably also pertinent to the structural flexibility of noncrystalline films.

Another important property of hydrogen (water) in passivating films is its role in self-repair as has been pointed out by Okamoto.[3]

This effect is somewhat analogous to the reduction of interface states (dangling Si bonds) at the Si/SiO_2 interface by forming Si-H or Si-OH bonds.[13] In this manner the reactive sites can be tied up so that the apparent perfection of the Si/SiO_2 interface is increased. However, this interface is more sensitive to destructive effects (e.g. irradiation) than a quasi-perfect Si/SiO_2 interface where practically all Si atoms are bonded to oxygen.

Hydrogen may be present even in films grown at high temperatures under relatively clean conditions; for example, SiO_2 films or silicon may contain SiOH and/or SiH groups up to 10^{22} cm^{-3}.[28] Evidently, a very high concentration of hydrogen is to be expected in thin passivating films formed at room or in aqueous environments. In this respect, hydrogen should be considered as a major constituent for these films rather than an "additive". This is a very important area for detailed studies.

3.2 Substrate Effects

The difference in the oxidation behavior of polycrystalline Ta foil and vacuum deposited Ta film on silicon, described above, demonstrates that the substrate influences the structure of the oxide film. In this particular case, the Ta film was also polycrystalline but the crystallite size was very small (~100A) and the film was porous. Even so, vitreous oxide films formed. A substrate effect was observed even with SiO_2 films: oxide films grown on sandblasted single crystal Si surface had crystallites, whereas the film grown on smooth surfaces were vitreous.[11] The most significant substrate effect is the tremendously increased corrosion resistance (by 5-6 orders of magnitude) of amorphous metals relative to polycrystalline metals of identical composition to be discussed below. Substrate effects are probably involved in the enhanced corrosion resistance of pure iron which was implanted with Ar ions.[29] This was attributed to the thickening of the air-formed oxide film as inferred from electrometric reduction. However, it is possible that the structurally disturbed or even amorphous metal surface, resulting from the ion bombardment, behaves somewhat similarly to amorphous metals. As a result, a noncrystalline passivating film may form with greater ease. It is expected that, even when the main propose of ion implantation is to introduce an additive which improves the passivation behavior, some effects due to surface disordering in the metal structure will arise.

Crystal nucleation rate in the noncrystalline oxide film and, hence, the stability of the noncrystalline structure depend very much on the substrate. This indicates that the formation and stability of a noncrystalline film are determined by the balance between the competing processes of its growth and crystallization.

3.3 Thin Film Effects

An important, but frequently overlooked, point is the implications of the fact that passivating films are very thin. The usual

considerations derived from bulk behavior are not necessarily applicable to thin film phenomena. For example, PtSi can be formed at ~200°C by an interface reaction between Si substrate and thin (several hundred Angstroms) Pt film whereas, according to the phase diagram, the minimum temperature should be above 700°C.[30] Also, an oxidizing reaction due to oxygen diffusion through the Ta_2O_5 takes place at the Si/Ta_2O_5 interface at a temperature which is not sufficiently high to oxidize bare silicon.[15] Kinetic rather than thermodynamic considerations are crucial in thin film phenomena where the interface energy is often high and overcomes other energy barriers.

These "thin film effects" further complicate the situation in noncrystalline oxide films which is already complicated due to the lack of crystallinity. The structural information obtained from x-ray or electron diffraction is not enough to characterize these films. There is a great need for using techniques which give information on short-range order and on the nature of the chemical bonds. These studies should complement electrochemical measurements. The complexity arising from the thinness of passivating films and from their noncrystalline structure can be unraveled only by using sophisticated techniques and, just as importantly, sophisticated and unconventional concepts and ideas.

4. NONCRYSTALLINITY AND PASSIVITY

There are various indications that the special properties of noncrystalline films described above affect the formation stability and repairability of passive films. It will be the task of this section to examine the evidence that noncrystalline films provide more "perfect" passive films.

4.1 Formation of More Protective Passive Films

Both the rate of growth and the limiting thickness of passive films should be affected by the degree of crystallinity. This is so because these factors are dependent on the ability of anions or cations to move through the growing film. As pointed out earlier, this retardation in ionic mobility occurs because noncrystalline films have few defects or grain boundaries that enhance ionic movement. There are a number of experiments that can be interpreted as supporting this concept.

First, consider a situation where an alloy forms a noncrystalline film. An example is the Fe-Cr alloys shown by McBee and Kruger[2] to form noncrystalline films on more and more surface grain orientations as the Cr content goes up. In Table I is shown a comparison of the limiting thicknesses formed in the passive potential region on alloys containing different Cr contents. It can be seen that with increasing Cr and the increasing noncrystallinity of the passive film, the limiting film thickness is decreasing. Moreover, as the thickness of the passive film that forms on an alloy surface is decreased, its ability to protect that surface increases. High chromium alloys are, of course, more corrosion resistant than are low chromium ones.

As was mentioned above, amorphous alloys exhibit remarkable corrosion resistant behavior.[31] For example, Hashimoto et al.[31] have shown that the passive current for an amorphous Fe-Cr-P-C alloy is over two orders of magnitude lower than that for the same alloy that has been converted from a metal glass to the usual crystallized metal. Such superior ability to lower the passive current density must reside in the superior ability of the film formed on the metal glass to decrease the flow of ions.

As discussed earlier above, hydrogen appears to play a beneficial role in affecting the properties of noncrystalline films or their ability to form. For example, Ti forms a much more protective film in wet oxygen as compared to the film formed in dry oxygen.[4] A number of workers have provided evidence for hydrogen or "bound water" in both crystalline and noncrystalline passive films.[3],[32] For example the passivity associated with the outer layers of the passive film on iron was found to depend on the role of hydrogen in promoting the formation of the crystalline γ-Fe_2O_3.[33] Therefore, the role of hydrogen may not be only related to the promotion of noncrystallinity or its effect on the structure of noncrystalline films.

4.2 Resistance to Breakdown

Just as noncrystallinity appears to have some beneficial effect on the formation of a more protective film in the passive region of the anodic polarization curve, there are also indications that when a metal is at a potential above the critical potential for pitting, the ability to resist breakdown leading to pitting or crevice attack is enhanced by the existence of a noncrystalline film on its surface. Fig. 1 shows a comparison between the breakdown behavior on Fe (crystalline film) and on Fe-Cr (noncrystalline film). The superiority of the noncrystalline film with regard to resistance to breakdown is reflected in its greater time for breakdown even while being thinner and being exposed to higher concentrations of damaging species (chloride ions). Also of great interest is the finding that for the crystalline passive films on Fe, one can remove Cl^- ions from the film by replacing the chloride containing solution with one that does not contain chloride, whereas for the noncrystalline films on Fe-Cr, the Cl^- cannot be removed in a similar fashion. Therefore, noncrystalline films resist breakdown by making entry by damaging species more difficult, but they also inhibit exit once some penetration has taken place. This would imply that whereas entry or exit of Cl^- occurs via defects or grain boundaries in crystalline films, it may only enter the noncrystalline films by becoming part of their "glass-like polymeric" structure. Such stable structures, as the results in Fig. 1 show, are both difficult to enter and difficult to exit.

Similarly, the breakdown of a film in a crevice is affected by the crystallinity of the passive film. Fig. 2 shows results using an optical technique described elsewhere.[36] It shows that as one increases the Cr content, the tendency to breakdown as reflected by the change in the

optical parameter, Δ, (relative phase retardation) is retarded. Ambrose and Kruger[36] have attributed this decrease in Δ to the onset of conditions in a crevice that lead to breakdown.

Two other indications that passive film crystallinity can affect breakdown are provided by the work of Devine and Wells[37] and Okamoto[3]. The former observed that no pitting occurred because of breakdown of the films on amorphous metals, presumably (our interpretation) because these films were noncrystalline. Once the metals were crystallized by heat treatment, however, pitting took place, presumably because the films formed on the crystalline substrate were no longer crystalline. Okamoto showed that the induction time for pitting of an austenitic stainless steel could be decreased if its noncrystalline film were annealed. This behavior is exactly the opposite to that found for iron by Ambrose and Kruger[38] who found that annealing increased the time to breakdown (induction time for pitting). A plausible explanation for these opposite behaviors is that annealing promotes crystallization of the noncrystalline film on the austenitic stainless steel, making breakdown easier by providing more paths for Cl^- ingress. For the crystalline film on Fe, however, annealing removes defects such as cation vacancies and thereby makes ingress of Cl^- and thus breakdown more difficult.

4.3 Ductility

The last section was concerned with chemical breakdown. There is also the possibility of mechanical breakdown —— the rupture of passive films by applied stress. This form of breakdown is of great importance for stress corrosion cracking of metals. Noncrystallinity of passive films can play an important role affecting this kind of breakdown through its influence on the ductility of the film. A more ductile film would have a better chance for avoiding mechanical breakdown. Vermilyea[39] has stated, for example, that stress corrosion cracking is not possible if the passive film is plastically ductile. It should be pointed out also that some theories of chemical breakdown leading to pitting also postulate film rupture by chemical forces[40], and thus ductility may be important for all forms of breakdown.

There are some indications in the literature that degree of crystallinity does affect film ductility. Bubar and Vermilyea[41] showed that anodic Ta_2O_5 films lost their ductility after crystallization. Bubar and Vermilyea[42] also have shown that there is a wide variation in the ductility of passive films formed on a number of metals. Films formed on Ta, which is known to form noncrystalline films, exhibited deformations of as much as 50% before fracture. Also, the passive film on 304 stainless steel (noncrystalline) exhibited better ductility than that on crystalline iron. Aluminum, which may or may not form noncrystalline films, formed films less ductile than those on Fe. Leach and Neufeld[43], however, found easy deformation of films on Al under an applied field. It is thus not certain that the ductility of passive films can only be attributed to noncrystallinity. Other factors such as the presence of hydrogen in the film may also play a complicating role.

4.4 Repassivation

When breakdown occurs, repassivation rate can play an important role in determining whether passivity can be restored or whether localized attack such as cracking, pitting or crevice corrosion can be initiated. There are no direct experiments to our knowledge that indicate that noncrystalline films reform at a greater rate than crystalline ones do, but one can obtain indications of this if one compares the repassivation of low carbon steel (crystalline film) to austenitic stainless steel (noncrystalline film). Using the technique of tribo-ellipsometry[44,45], Ambrose and Kruger have obtained repassivation ratios, Rp, for these metals. Rp is a measure of the efficiency of repassivation; it is the ratio of the total current during repassivation (the current consists of both dissolution and film growth components) to the thickness of the reformed passive film for a given instant of time during the repassivation event. Fig. 3 shows that the time of repassivation and the magnitude of Rp are considerably lower for the stainless steel than they are for low carbon steel. These results thus indicate that the rate of passive film regrowth and the effectiveness of retarding metal dissolution are enhanced for alloy surfaces that form non-crystalline films.

5. CONCLUSIONS

Owing to the lack of grain boundaries, noncrystalline oxide films have better passivating properties than polycrystalline ones. Bond and/or structural flexibility is an important factor in determining the ability to form a noncrystalline structure and its stability: This point was demonstrated by the example of vitreous SiO_2 and Ta_2O_5 as well as by ligand formation of transition metal ions. The flexibility of the noncrystalline structure ensures a good accommodation at the oxide/substrate interface without requiring an epitaxial relationship. Such an interface is less prone to chemical attack than an imperfect one. High degree of short range order in vitreous oxide films also contribute to their chemical resistance. The flexibility of the structure is responsible for the increased ductility of noncrystalline passivating films which is crucial from the viewpoint of pitting and stress corrosion.

The structural/bond flexibility and, hence, the tendency toward noncrystallinity can be increased by additives; the effect of Cr in the passivation behavior of stainless steel is an example. In this respect, hydrogen also plays a great role by forming M-OH groups, hydrogen bonds, and H_2O ligands.

The formation and stability of noncrystalline oxide films is a kinetic rather than thermodynamic problem as demonstrated, for instance, by the influence of substrate. Due to the increased stability of noncrystalline passivating film, amorphous alloys exhibit orders of magnitude greater corrosion resistance than the polycrystalline alloys of identical composition.

Thermodynamic and other concepts used in connection with bulk crystalline solids are not a priori applicable to thin and non-crystalline passivating films. Many aspects of thin noncrystalline films are determined by unique interface reactions and unique properties of a noncrystalline structure.

There is evidence in the literature that noncrystalline passive films are 1) more protective, forming films which exhibit lower limiting thicknesses and lower passive current densities; 2) more ductile, 3) less susceptible to breakdown by damaging species and 4) capable of reforming at greater repassivation rates than crystalline films.

ACKNOWLEDGEMENTS

The contribution to this paper of A.G. Revesz is based upon work performed in COMSAT Laboratories under the sponsorship of the Communications Satellite Corporation. The contribution of J. Kruger was supported by the Office of Naval Research under contract NAONR 18-69 NR036-082.

Thanks are due to F. Fehlner for helpful comments on the manuscript.

References

1. T.P. Hoar, J. Electrochem. Soc. 117, No. 1, p. 17C (1970).

2. C.L. McBee and J. Kruger, Electrochem. Acta, 17, 1337 (1972).

3. G. Okamoto, Corrosion Science 13, 471 (1973).

4. J.S.L. Leach, Surface Science 53, 257 (1975).

5. F.P. Fehlner and N.F. Mott, Oxidation of Metals 2, 59 (1970).

6. W.H. Zachariasen, J.Am. Chem. Soc. 54, 3841 (1932).

7. K.R. Lawless, Repts. Progr. in Physics 37, 231 (1974).

8. M.J. Pryor, Oxidation of Metals 3, 271 (1971).

9. L. Young, Anodic Oxide Films, Academic Press, New York (1961).

10. P.J. Harrop and D.S. Campbell, Thin Solid Films 2, 273 (1968).

11. A.G. Revesz, Phys. Stat. Soc. 24, 115 (1967).

12. M.M. Atalla, E. Tannenbaum, and E.J. Scheibner, Bell System Technical J. 30, 749 (1959).

13. A.G. Revesz, J. Non-Cryst. Solids 11, 309 (1973).

14. A.G. Revesz, J. F. Allison and J.H. Reynolds, COMSAT Technical Review, 6, 57 (1976).

15. A.G. Revesz and T. Kirkendall, J. Electrochem. Soc. 123, 1514-1519.

16. F.P. Fehlner, J. Electrochem. Soc. 119, 1723 (1972).

17. R.L. Myuller, in Solid State Chemistry (O.U. Borisova, ed.), translated from Russian, p. 1, Consultants Bureau, New York, (1966).

18. C.S.G. Phillips and R.J.P. Williams, Inorganic Chemistry, Vol. 1, p. 480 and Vol. 2, pp. 189-239, Oxford University Press, New York, (1965).

19. P. Kofstad, High Temperature Oxidation of Metals, J. Wiley, New York (1966).

20. N.C. Stephenson and R.S. Roth, Acta. Cryst. B27, 1037 (1971).

21. R.S. Roth and J.L. Waring, J. Res. NBS 74A, 485 (1970).

22. J.S. Anderson, J. Chem. Soc. (Dalton), 1973, p. 1107.

23. B.G. Hyde, A.N. Bagshaw, S. Anderson, and M.O. Keeffe, in Annual Review of Materials Science, Vol. 4 (R.A. Huggins et al, eds.); p. 43, 1974.

24. A.F. Wells, Structural Inorganic Chemistry, p. 459 Clarendon Press, Oxford, 1975.

25. V. Ashworth, W.A. Grant, and R.P.M. Proctor, Corrosion Science 16, 661 (1976).

26. A.F. Wells, op.cit., pp. 526-529.

27. C.S.G. Phillips and R.J.P. Williams, op. cit., Vol. 1, p. 533.

28. A.G. Revesz, J. Electrochem. Soc., in press.

29. V. Ashworth, W.A. Grant, R.P.M. Proctor, and C. Wellington, Corrosion Science, 16, 393 (1976).

30. W. Mayer and K.N. Tu, J. Vac. Sci. Tech. Vol. 11, 1074.

31. K. Hashimoto, K. Osada, T. Masumoto, and S. Shimodaira, Corrosion Science 16, 71 (1976).

32. H.T. Yolken, J. Kruger and J.P. Calvert, Corrosion Science, 8, 103 (1968).

33. C.L. Foley, J. Kruger, and C.J. Bechtoldt, J. Electrochem. Soc. 114, 944 (1967).

34. C.L. McBee and J. Kruger, Nature Physical Sci. 230, 194 (1971).

35. C.L. McBee and J. Kruger, Proceedings Japan-U.S.A. Symposium on Passivity and Breakdown of Passivity of Iron Base Alloys, R.W. Staehle and H. Okada, eds., National Association of Corrosion Engineers, Houston, 1976, p. 131.

36. J. Kruger and J.R. Ambrose, Nat. Bureau of Standards Report NBSIR 74-583, Sept. 1974.

37. T.M. Devine and L. Wells, Scripta Metallurgia 10, 309 (1976).

38. J.R. Ambrose and J. Kruger, Proc. 4th Int. Cong. on Metallic Corrosion, National Association of Corrosion Engineers, Houston, 1972, p. 698.

39. D.A. Vermilyea, Physics Today, 29, 23 (1976).

40. J. Kruger, see Ref. 35, p. 91.

41. S.F. Bubar and D.A. Vermilyea, J. Electrochem. Soc. 114, 882 (1967).

42. S.F. Bubar and D.A. Vermilyea, J. Electrochem. Soc. 113, 892 (1966).

43. J.S.L. Leach and P. Neufeld, Corrosion Sci. 9, 225 (1969).

44. J.R. Ambrose and J. Kruger, J. Electrochem. Soc. 121, 599 (1974).

45. J.R. Ambrose and J. Kruger, Proc. Fifth Int. Cong. on Metallic Corrosion, National Association of Corrosion Engineers, Houston, 1974, p. 406.

Figure Captions

Figure 1. (a) Spectro-ellipsometric measurements of changes in Δ, relative phase retardation, and Ψ, relative amplitude reduction, for iron after introduction of 0.005N chloride (t=0), and removal of chloride from the solution. Δ, Ψ, and current are seen to return to normal passive values once chloride ion is removed. 410 nm wavelength light was used. From (34).

(b) Spectro-ellipsometric measurements of changes in Δ and Ψ for Fe-20 Cr after introduction of 0.08N chloride (t=0), and removal of chloride from solution. Δ and Ψ do not return to passive values once chloride ions are removed. 450 nm wavelength light was used. From (35).

Figure 2. Changes in relative phase retardation, $\delta\Delta$, as a function of time measured within a crevice, using a glass plate to produce the crevice for Fe-14%Cr and Fe-17%Cr alloys exposed to 1N NaCl solution. From (36).

Figure 3. Comparison between the variation in Rp (repassivation ratio determined by triboellipsometry) in 1 N NaCl for 304 stainless steel (From 36) and low carbon steel (From 45).

TABLE I - Variation in Limiting Film Thickness As A Function of Chromium Content (from Ambrose and Kruger, unpublished) In Iron Chromium Alloys and Crystallinity of The Passive Films Formed On These Alloys (from 2).

% Cr	Degree of Crystallinity of Passive Film	Limiting Film Thickness (Å)
0	Well oriented spinel	36
5	Well oriented spinel	27
12	Poorly oriented spinel	21
19	Mainly non-crystalline	19
24	Completely non-crystalline	18

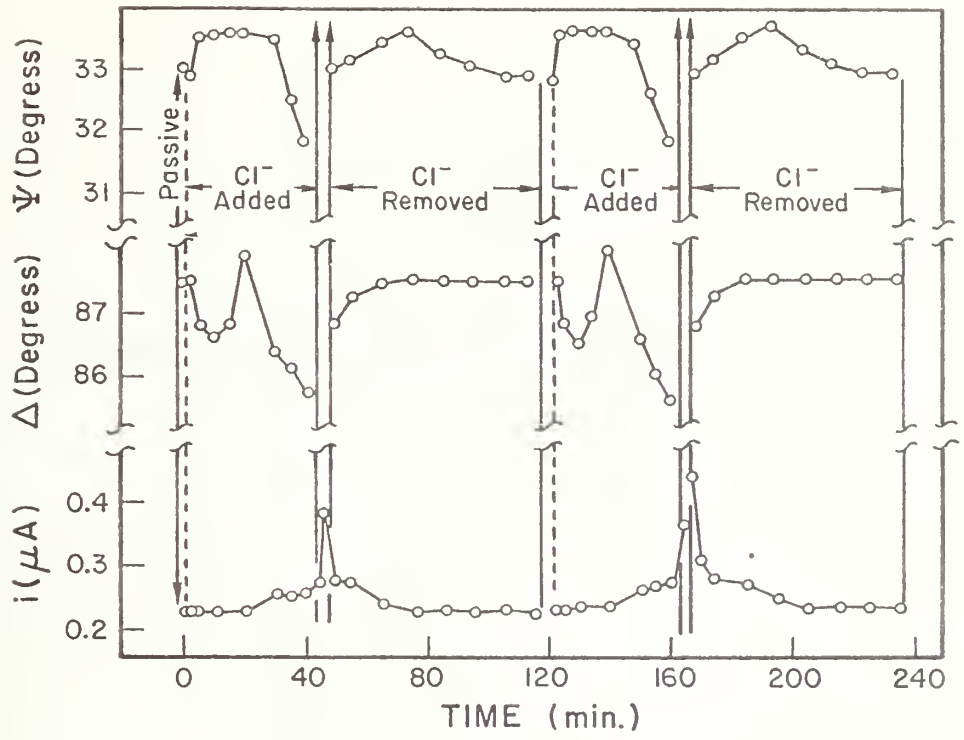
Ψ (Degress)
33
32
31
Passive
Cl⁻ Added
Cl⁻ Removed
Cl⁻ Added
Cl⁻ Removed
Δ (Degress)
87
86
i (μA)
0.4
0.3
0.2
0
40
80
120
160
200
240
TIME (min.)

(a)

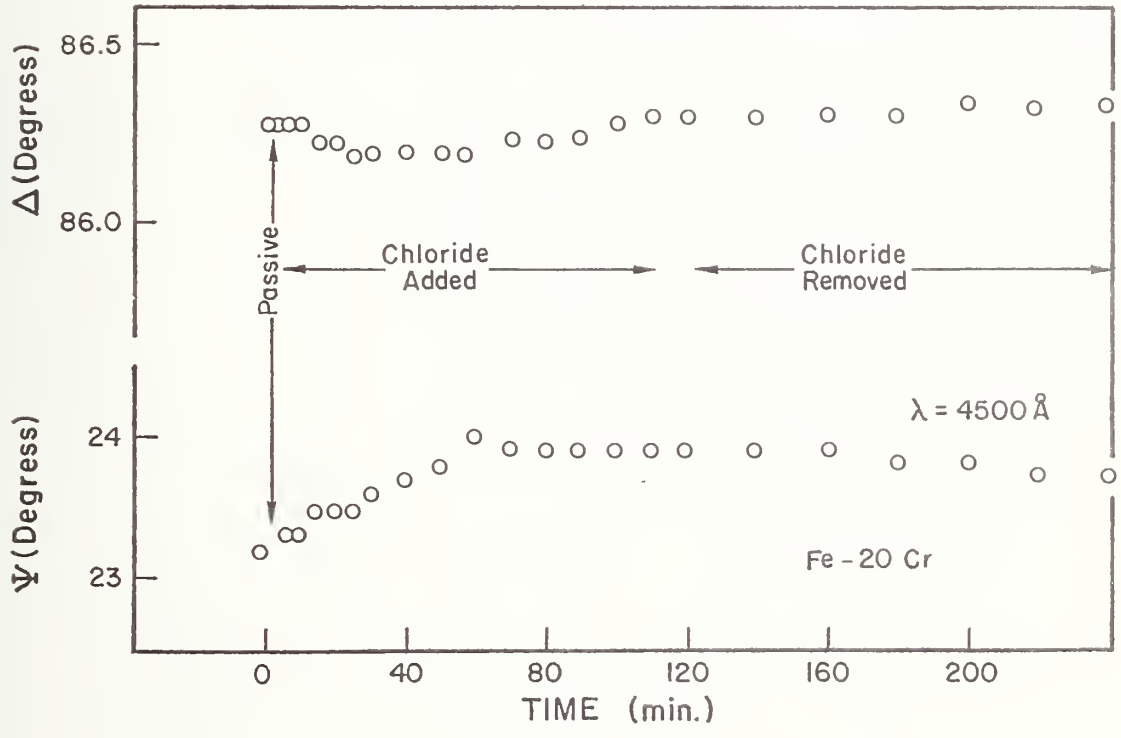
Δ (Degress)
86.5
86.0
Passive
Chloride Added
Chloride Removed
Ψ (Degress)
24
23
λ = 4500 Å
Fe - 20 Cr
0
40
80
120
160
200
TIME (min.)

(b)

Fig 1

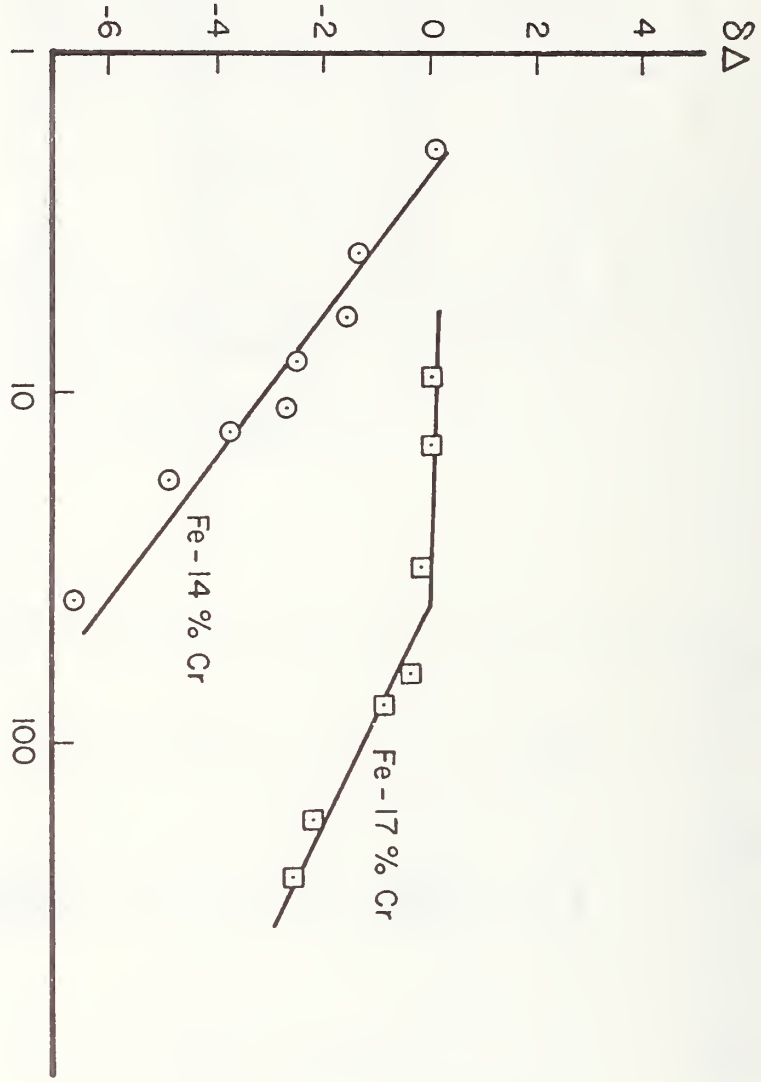

Fig 2

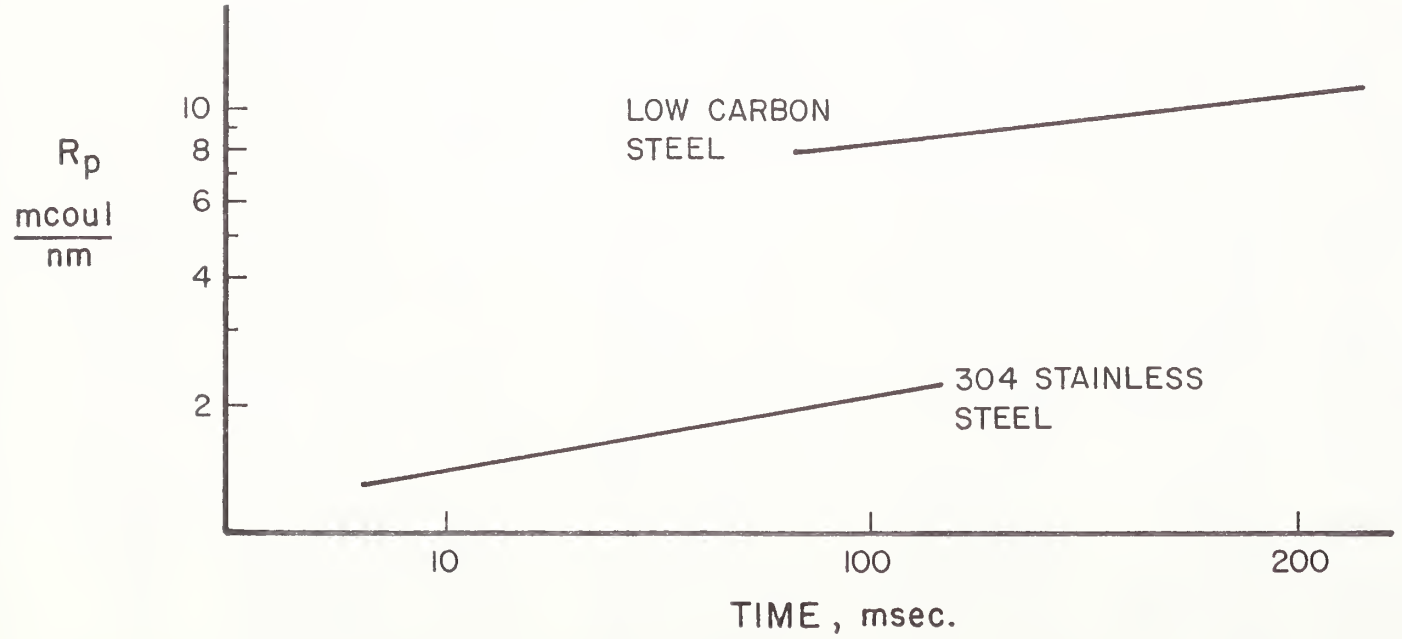
R_p
mcoul
nm
10
8
6
4
2
LOW CARBON
STEEL
304 STAINLESS
STEEL
10
100
200
TIME , msec.

Fig 7

PART III
To be submitted to Corrosion J.

Effect of Chromium Depletion on the Repassivation Kinetics of 18-10 Austenitic Stainless Steel in Sodium Chloride Solutions

John R. Ambrose
National Bureau of Standards
Institute for Materials Research
Washington, D. C. 20234

A great deal of effort has been directed toward obtaining an understanding of the relationship that appears to exist between the susceptibility of AISI 304 austenitic stainless steel for intergranular stress corrosion cracking (ISCC) and the tendency for this particular alloy to become sensitized as a result of welding operations. The importance of this relationship has been demonstrated upon careful analysis of the phenomonology of failures of AISI 304 pipe material exposed to high purity water in BWR nuclear reactor systems (1). In these systems, failure occurred either in the heat affected zones (HAZ) of weldments or in severely furnace sensitized material.

Although it is but one of several suggested mechanisms, the idea that the occurrence of carbides in grain boundaries as a result of improper heat treatment can be related to the phenomenon of sensitization is most interesting. The formation of these metallic carbides is presumably associated with a corresponding depletion in chromium in areas immediately adjacent to the grain boundaries where the particles have formed. Depletion of chromium to concentrations below that required to sustain passivity would account for many of the properties which have been displayed by material which has been sensitized.

However, the relationship between ISCC and sensitization becomes more complex if it is considered that sensitization appears to be a necessary but not sufficient criteria for controlling susceptibility of AISI 304 stainless steel to ISCC. This conclusion arises from the fact that out of some 17,000 welds, less than 100 have experienced any failure. Thus, techniques which measure only degree of sensitization will not necessarily yield information by which susceptibility to ISCC can be ascertained (i.e. ASTM Standard Procedure A-262, practices A, C, and E). Another parameter which has been shown to be related to the susceptibility of a material to stress corrosion cracking is the rate at which a bare metal surface will repassivate in the environment to which it has been exposed. The rationale behind this relationship of SCC to repassivation kinetics is incorporated into the mechanism described in other publications (2, 3).

It has been known for some time that overall corrosion resistance of stainless steels is related to the concentration of chromium in the alloy and that a minimum concentration of chromium (approximately 12%) is required to maintain a passive condition. It also has been shown that a relationship does exist between repassivation kinetics and susceptibility to SCC for AISI 304 austenitic stainless steels (4). What is not known, however, is what relationship exists between 1) chromium depletion of austenitic stainless steels and repassivation kinetics in solutions known to cause SCC and between

2) sensitization and repassivation kinetics in these environments. This paper describes the results of a study into the effect of chromium depletion on the repassivation kinetics of Fe-18Cr-10Ni austenitic stainless steels.

Experimental

As described in a previous report (5), a series of ternary Fe-10Ni-xCr alloys were prepared where x was varied between 3 and 18 weight percent in increments of 3%. Although considerable effort was expended to retain the austenite structure in these alloys, the final structure in all specimens other than 18%Cr was a martensite-like phase dispersed in a ferritic steel matrix. There is, of course, the question as to what effect the alteration of structure would have on repassivation kinetics of a particular alloy composition but this will have to be determined at a future time. These studies should, however, provide insight into how alloy composition is related to repassivation kinetics.

Cylindrical segments were cut from the prepared rod material and mounted in a Buehler expoxy mount. The finished specimens were drilled and trapped for electrode assembly. Repassivation kinetics were determined using a modification of the tribo-ellipsometric technique in which the anodic current decay was recorded as a function of time on an oscilloscope. All experiments were performed in a 1.0N NaCl solution in which no attempt was made to deaerate the system. Measurements were made for each alloy at its respective corrosion potential and at several other more noble potentials, including values above the critical pitting potential of that particular alloy.

The experimental procedure in each instance was the same: After electrode installation in the electrochemical cell and connection of electronic leads, solution was added to the cell and the rest potential allowed to stabilize. The tribo-ellipsometric abrasion apparatus was activated and the metal surface abraded for approximately 5 seconds following which the abrasion wheel was retracted and repassivation was monitored by recording the current decay transient on an oscilloscope. The process was repeated for a given alloy potentiostatted at several more noble potentials. Solution was changed for each alloy and the experimental procedure repeated.

Results and Discussion

In figure 1 are plotted current decay against time for the Fe-18Cr-10Ni alloy at several potentials. Current decay kinetics were virtually independent of applied potential. In Figure 2 are plotted results from repassivation kinetics of Fe-15Cr-10Ni alloy. Initial current decay kinetics are independent of potential, but above the critical pitting potential, at 249 mV SHE, current decay abruptly slows as onset of pit growth begins. Results are not shown for the Fe-12Cr-10Ni alloy since the measured currents at the corrosion potential were inconsistent with results obtained from other alloys. Microscopic inspection of the specimen surface revealed crevice corrosion attack at the interface between the metal and the expoxy mounting resin due probably to an imperfect seal of mount to metal. Results of experiments in which this alloy has been tested will be presented in future work.

In Figure 3 are plotted the current decay kinetics for the 9% chromium alloy. In this case, there is a marked difference in the potential dependence of the repassivation rate. This effect is particularly pronounced as the potential is increased from 150 to 250mV SHE. Above 250mV, the critical potential for pitting is exceeded. At 350mV, after about 45 milliseconds there is an abrupt increase in the rate of current decay. This effect is probably due to formation of corrosion product at the solution interface which restricts anodic dissolution.

Figure 4 shows the repassivation kinetics for the 6% alloy. Current decay kinetics for this and the 3% alloy (figure 5) are markedly decreased Again, as for the 9% alloy, there is a potential dependence exhibited for the rate of current decay. In addition, at the higher applied potential, there is an inflection in the current decay plot at 165 mV at about 32 ms. A similiar increase in the rate of current decay is noted for the 3% alloy at 9mV and 25ms. It is interesting to note that the point in time at which these inflections occurred in the 9, 6, and 3% alloys corresponds to approximately the same quantity of consumed change for each alloy, $\sim$0.5 coulombs. This would further support the view that repassivation is due in part to the formation some insoluble substance, which precipitates at the metal surface when the solubility product of that substance has been exceeded.

In Figure 6 are compared repassivation rates for the 18, 15, 9, 6 and 3% alloys at their respective open circuit or corrosion potentials. It is immediately obvious that repassivation is exceptionally difficult for the 6 and 3% alloys. The difference in repassivation rates becomes much more pronounced under anodic polarization. In Figure 7 are compared current decay kinetics for all alloys of the series at a given applied potential of 142mV SHE. From this plot, the set of alloys can be divided into three groups based upon their rates of repassivation: group I - 18, 15, 12% Cr, fastest repassivation kinetics; group II - 6, 3% Cr, slowest repassivation kinetics; and group III - 9% Cr; intermediate repassivation rates.

From these results it appears likely that the rate of repassivation of this family of stainless steels is proportional to the concentration of chromium in the alloy. It is particularly worthwhile to note that an area of intermediate repassivation kinetics does exist, between 12 and 6% chromium. This is interesting because such an intermediate value of repassivation rate has long been suggested as being a criteria for propagation of sharp cracks during ISCC.

The fact that an intermediate region of passivation behavior exists also explains why sensitization is considered a necessary but not sufficient condition for susceptibility to ISCC. Areas of the heat affected zone must be of a certain chromium concentration (degree of sensitization) and in an area of the metal where metallurgical factors are such that crack advance is favored.

Of secondary interest is the observation that, under conditions of restricted repassivation by the original passive film, current decay is apparently affected by the formation of another substance at the metal surface. Perhaps as has been previously suggested, this substance is a salt film of limited solubility under these conditions of repassivation.

Two considerations should be made in treating the results obtained from this study to date:

1) The technique does allow detection of intermediate values of repassivation behavior. Techniques based upon an analysis of time to failure or examination of a current-potential plot will not permit such detection since the measured parameters are based upon a cumulative series of events. No one step of the process can be isolated from the rest. By using a technique based on repassivation as being the most important step in controlling ISCC susceptibility, measurement of a parameter which is directly related to the repassivation kinetics of exposed metal will provide a more meaningful diagnostic tool.

2) Although the technique can be used to detect values of the chromium concentration where an alloy becomes susceptible to ISCC, it is not known at this time if differences in repassivation kinetics can be measured when the chromium depletion is restricted to minute areas at the surface of the specimen - i.e. adjacent to the grain boundaries of a polycrystalline material. Specimens have been produced in which the material has been heat treated to several degrees of sensitization. Results of their measured repassivation kinetics should answer the question.

Conclusion

1) Repassivation kinetics of Fe-Cr-Ni stainless steels are affected by variations in the chromium concentration of the alloy.

2) There exists an intermediate range of repassivation behavior between 12 and 6% chromium concentration which may be tied to the question of how sensitization and susceptibility to ISCC are related.

3) Even though chromium depletion is related to repassivation kinetics, it is not known whether this technique can detect variations in the repassivation kinetics of material which has been heat treated to different degrees of sensitization. These results will be the subject of the next report.

References

1. NEDG-21000, Report prepared for Electric Power Research Institue by A.J. Giannuzzi, General Electric Project Engineer, BWR Reactor Systems Department.

2. J. R. Ambrose and J. Kruger, Corrosion 28. 30 (1972).

3. J. R. Ambrose and J. Kruger, J. Electrochem. Soc. 121, No. 5., 599 (1974).

4. Office of Naval Research, NAONR 18-69 NBS Report No. NBSIR 74-583, September 1974.

5. Ibid., NBS Report No. NBSIR 76-1170, November 1976.

Figure Captions

Figure 1. Plot of anodic current in milliamperes versus time in milliseconds for Fe-18Cr-10Ni in 1.0 N NaCl solution at 118, 218, 518 mV SHE.

Figure 2. Plot of anodic current in milliamperes versus time in milliseconds for Fe-15Cr-10Ni in 1.0 N NaCl solution at -51, 49, and 249 mV.

Figure 3. Plot of anodic current in milliamperes versus time in milliseconds for Fe-9Cr-10Ni in 1.0 N NaCl solution at 150, 250, and 350 mV.

Figure 4. Plot of anodic current in milliamperes versus time in milliseconds for Fe-6Cr-10Ni in 1.0 N NaCl solution at -35, 65, 165 mV SHE.

Figure 5. Plot of anodic current in milliamperes versus time in milliseconds for Fe-3Cr-10Ni in 1.0 N NaCl solution at -91 and 9 mV SHE.

Figure 6. Comparison of repassivation kinetics for series of Fe-XCr-10Ni (x= 18, 15, 9, 6, and 3%) at their respective open circuit potentials.

Figure 7. Comparison of repassivation kinetics for series of Fe-XCr-10Ni (x= 18, 15, 12, 9, 6, 3%) at 142 mV SHE.

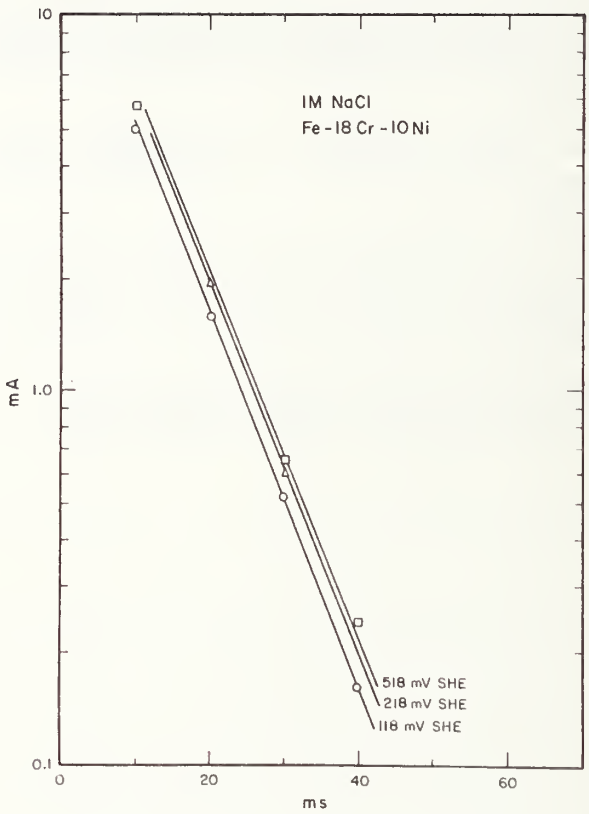
10
1.0
0.1
mA
0
20
40
60
ms
1M NaCl
Fe-18 Cr-10 Ni
518 mV SHE
218 mV SHE
118 mV SHE

Figure 1

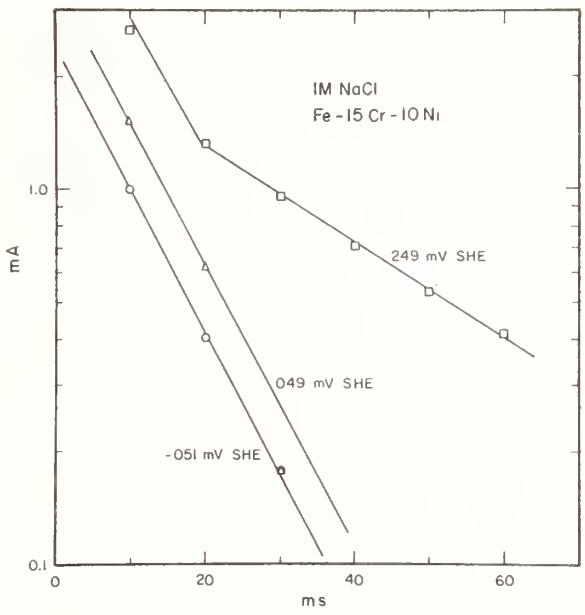
1M NaCl
Fe - 15 Cr - 10 Ni
249 mV SHE
049 mV SHE
-051 mV SHE
1.0
0.1
mA
0
20
40
60
ms

Figure 2

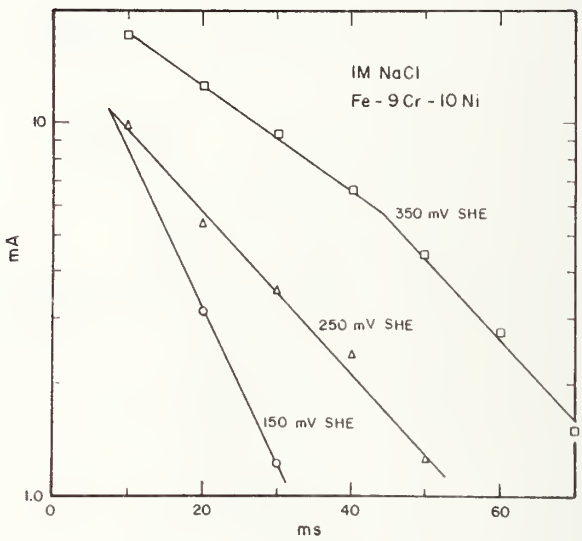
1M NaCl
Fe - 9 Cr - 10 Ni
350 mV SHE
250 mV SHE
150 mV SHE
10
1.0
mA
0
20
40
60
ms

Figure 3

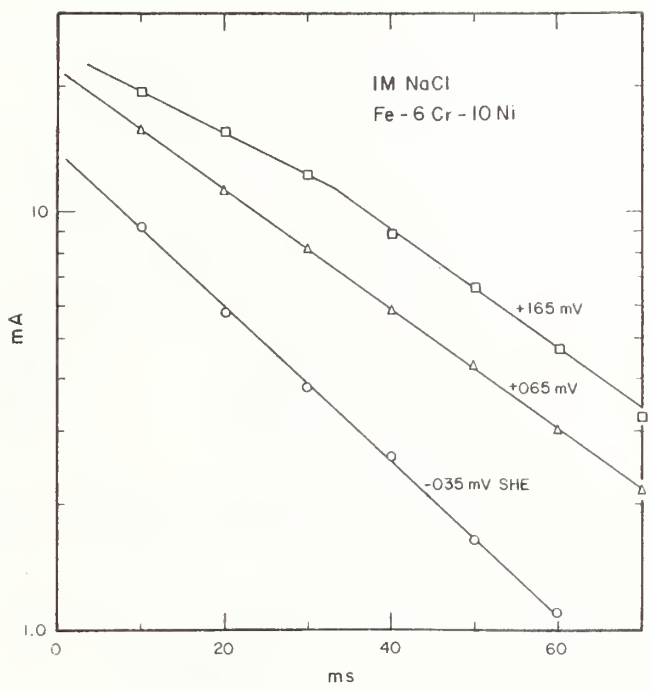

Figure 4

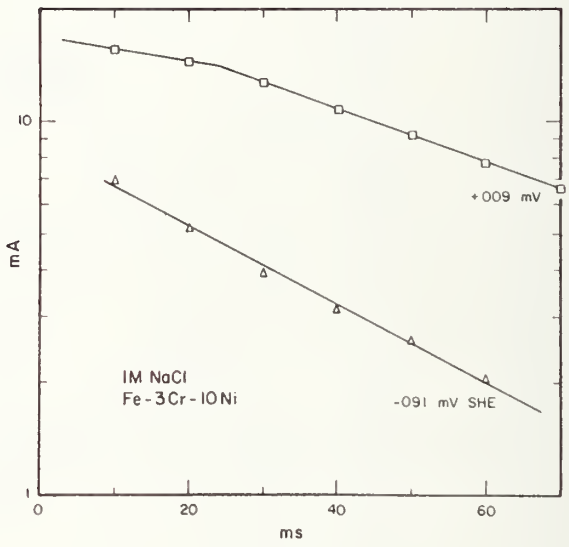

Figure 5

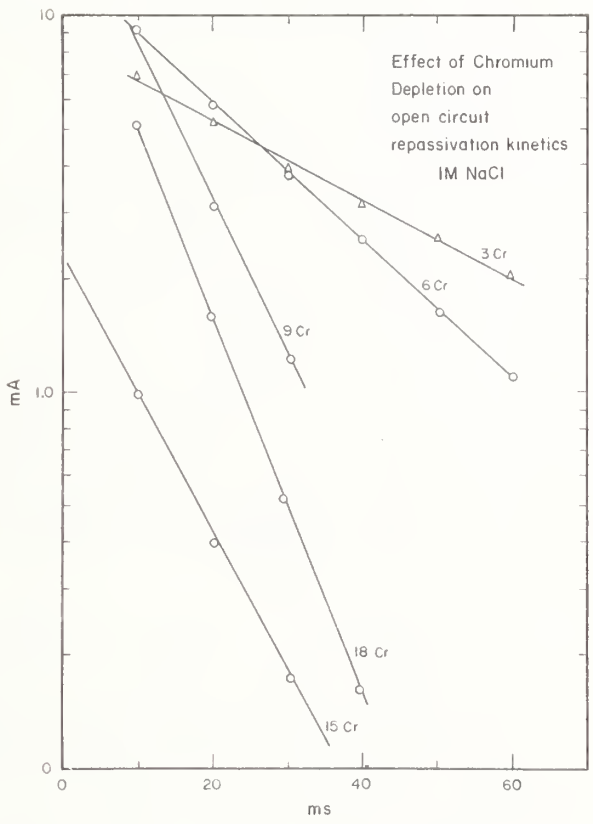
Effect of Chromium
Depletion on
open circuit
repassivation kinetics
1M NaCl
3 Cr
6 Cr
9 Cr
18 Cr
15 Cr
mA
10
1.0
0
0
20
40
60
ms

Figure 6

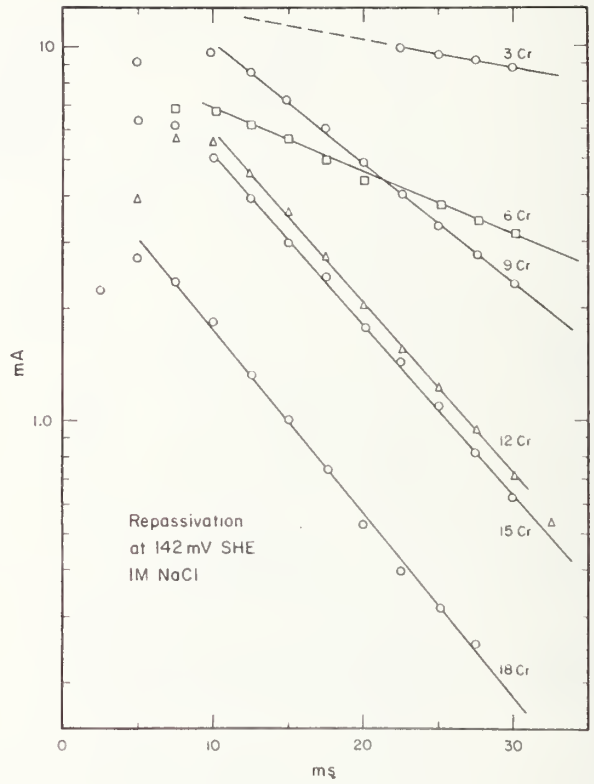
10
1.0
mA
0
10
20
30
ms
3 Cr
6 Cr
9 Cr
12 Cr
15 Cr
18 Cr
Repassivation
at 142 mV SHE
IM NaCl

Figure 7

PART IV To be published in Proceedings of 4th International Symposium on Passivity

Composition of Surface Films Formed During the Repassivation of Iron and Iron-Molybdenum Alloys

J. R. Ambrose
Institute for Materials Research
Metallurgy Division
National Bureau of Standards
Washington, D.C. 20234

Molybdenum has been in use for some time as an inhibitor of localized corrosion, both as an alloying addition and as a salt dissolved in the solution to which the metal is to be exposed. Although the phenomonology of the inhibition has been characterized, little progress has been made in developing a comprehensive understanding of the inhibition mechanism.

Recent spectroscopic surface profile analyses require new explanations for the influence of molybdenum on passivity and how this passivity is related to properties of surface films. Auger Electron Spectroscopy (AES) data have revealed an apparent surface depletion of molybdenum, which occurred in conjunction with an increased resistance to localized corrosion attack (1). One possible explanation has been developed from results obtained from a study into the effect of molybdate ion additions on pitting of iron in chloride solutions (2). Inhibition of propagation of pits appeared to be related to the accumulation, in repassivated pits, of molybdenum, which was thought to be in the form of an iron molybdate salt film. If formation of such a film were responsible for the resistance of iron to pit propagation in the presence of molybdates, then it is under those conditions of restricted mass transport that are most likely to exist during propagation of localized corrosion attack that such films would be expected to be the most stable and the most protective. In order to study repassivation under such conditions, a crevice electrode system with a window was conceived.

This system was designed so that simultaneous measurement of optical variations and electrochemical parameters could be made during the onset of crevice corrosion attack or during cathodic depassivation - anodic repassivation cycles within the crevice. However, location of the various electrodes-working, reference, and auxiliary - was such that current distribution has never been uniform over the exposed surface of the working electrode. Thus, until now, results have been limited to analyses of current decay curves obtained during repassivation transients. It was possible, though, even without obtaining measurement of film growth kinetics, to evaluate the contribution of alloyed molybdenum to the repassivation kinetics of iron in chloride solutions under the influence of a crevice and to speculate on the mechanistic implications.

Molybdenum affects the repassivation behavior of the alloys in two ways:

a) the initial rate of current decay is proportional to the concentration of molybdenum in the alloy and

b) the length of time during which the current continues to decrease is also proportional to the concentration of molybdenum in the alloy. Longer time intervals lead to lower values of crevice corrosion current during exposure.

Based on these electrochemical measurements, it was suggested that the stability of a molybdate salt film was a contributing factor to the repassivation kinetics of iron-molybdenum alloys and thus directly responsible for the observed improvement in corrosion resistance upon introduction of molybdenum into ferrous based alloys (4).

Critical questions remain - What is the nature of the repassivating film under conditions where crevice corrosion occurs, under what conditions does it form, and how fast does it grow? In order to answer the first question the crevice electrode was redesigned so that more uniform current distribution could be achieved. Following repassivation in an environment known to produce crevice corrosion, specimens were removed and the surfaces were analyzed by x-ray photoelectron spectroscopy (XPS) to determine film composition relative to the concentration of molybdenum in the alloy. An AEI ES 200 XPS spectrometer was used for these studies; analysis was performed by Nils E. Erikson of the Surface Science Division, National Bureau of Standards. The results of this study, when coupled with results presented in preceeding reports (2, 3), give some insights into the role of molybdenum as an inhibitor of corrosion.

Experimental

The crevice electrode assembly was virtually identical to that already described (3) except that the glass disc used to produce the crevice was coated on one side with a film of tin oxide. Silver epoxy was used attach a piece of platinum wire for electrical connection. The electrically conducting tin oxide served as an auxiliary electrode located within the crevice. This particular orientation of counter to working electrode, coupled with the position of the reference electrode within the crevice, permitted a better current distribution over the working electrode surface than has been achieved to date.

Specimens of Fe-1Mo and Fe-5Mo, machined from the same material described in previous reports (2, 3) to 2.5 cm x 0.15 cm x 0.62 cm, were so designed that they could be placed in the chamber of an XPS spectrometer. A section of teflon rod was slotted in one face to hold the specimens, then drilled and tapped to receive necessary electronic connections. Surfaces were polished through SiC papers to a 1 micron diamond paste finish. Spectra were obtained for both compositions before exposure to any solution; XPS scans were performed to determine composition at the surface of the air-formed film and again following argon ion sputtering to remove oxide films.

Specimens were then assembled in the crevice electrode system and exposed to an 8.41 pH borate buffer solution. Cathodic reduction at -758 mV SHE preceded repassivation at a potential of 442 mV SHE. Quantity of

repassivation was monitored coulometrically and, when 1.15×10^{-2} coulombs had been consumed, the potentiostat was turned off, the electrode disassembled as rapidly as possible, and the working electrode rinsed with spectro grade methanol and dried in a stream of compressed air. The specimens were removed from the teflon holder, wrapped in a piece of lens tissue, placed in a coin envelope, and transferred to the laboratory where the XPS analysis was performed.

Following analysis, specimens were repositioned in the teflon mounting adapter and returned to the electrochemical cell. This time, the solution used contained 10^{-2} M sodium chloride in the 8.41 pH borate buffer. The experimental procedure was identical to that described above. However, there was some over run in the charge consumed due to the decreased repassivation kinetics in chloride containing solution. The consistancy of the consumed charge for all experiments was within ±2%. Following solution exposure, XPS analysis was repeated.

Results

Compositions of Film on Fe-Mo Alloys

An XPS spectrum obtained from an air-formed film on molybdenum is shown in figure 1. By comparing Mo 3d peak positions in this spectrum with those in a spectrum obtained following film removal by argon ion (Ar^+) sputtering, it is possible to distinguish between elemental and combined molybdenum. As a first approximation, quantitative relationships were derived from calculation of peak height ratios of the respective states. For the two Fe-Mo alloys, quantitative results are presented in figure 2 as ratios of elemental iron and molybdenum to their respective combined states. Also presented in figure 2 are the ratios of total molybdenum to total iron. Mo/Fe peak height ratios for the oxide free surfaces (Ar^+) of the Fe-5Mo and Fe-1Mo alloys are themselves in a ratio of 5:1 (3.0 to 0.6) which indicates that the peak height measurement is appropriate for estimating surface composition ratios. In fact, the Mo/Fe ratios for the two alloys were in a 5:1 ratio for all surface conditions studied - in figure 2 these are denoted as:

Ar^+ - film free surface following Argon ion sputtering

Air film - air formed film following polishing

No (Cl) - anodic film grown in absence of chloride ion

(Cl) - anodic film grown in presence of chloride ion.

However, Mo/Fe ratios for the respective air formed films on each alloy were substantially less than in the substrate. As figure 2 shows, $(Mo/Fe)_{5Mo} = 2.2$, and $(Mo/Fe)_{1Mo} = 0.45$. This ratio decrease indicates a surface depletion in the amount of molybdenum relative to iron in the film.

This apparent molybdenum depletion is even more pronounced in anodic films grown in the absence of chloride iron. Mo/Fe ratios for Fe-5Mo and Fe-1Mo were 1.4 and 0.3, respectively. Furthermore, from figure

2, comparison of peak height ratios for elemental to combined states for both iron and molybdenum indicate that the anodic film is thicker than the air formed film.

The last set of results are from anodic polarization experiments in solutions containing 10^{-2} M NaCl. All ratios, $Fe_{(m)}/Fe_{(ox)}$, $Mo_{(m)}/Mo_{(ox)}$, and Mo/Fe, have increased in value over those from experiments in which no chloride was present in the solution. The ratios all approach those values determined for the respective air-formed films. It should be remembered that in these chloride containing solutions, repassivation rates for each alloy were substantially less than in non-chloride environments.

Bonding Characteristics of Molybdenum in Films on Fe-Mo Alloys

A comparison of the spectra for air-formed film to the anodic film on Fe-5Mo obtained following repassivation without chloride ion is given in figure 3. Notice the appearance of a peak intermediate between the two higher kinetic energy peaks as well as a disappearance of a low kinetic energy peak at the left side of the spectrum.

Since results shown in figure 2 indicate a large molybdenum depletion in the anodic film on these alloys, the spectrum obtained for the anodic film on Fe-5Mo grown without chloride ion could reflect the depletion of high oxidation state (+6) molybdenum compounds. However, when the spectrum obtained for an anodic film grown on Fe-5Mo in 10^{-2}M Cl^- is compared to that obtained for the air-formed film (figure 4), a return to the characteristics of the air-formed film is noted. As noted in figure 2, this change in the XPS spectrum for the anodic film is accompanied by an increase in the amount of molybdenum relative to iron.

Chloride in Films on Fe-Mo Alloys

The chloride absorption peaks for both alloys following repassivation in chloride solution at 442 mV SHE are compared in figure 5. There is substantially more chloride present in the Fe-5Mo alloy than in the 1Mo alloy. It should also be noted, however, that the ratio of peak heights for chloride is not in the same ratio as the concentrations of molybdenum - i.e. not 5:1. Rather, the ratio appeared to be about 2:1.

Discussion

Results obtained indicate a synergistic relationship between molybdenum and chloride ion during the repassivation of iron and iron-molybdenum alloys. Previous studies have been shown that molybdenum has little effect on the repassivation of iron whether in the form of an alloying addition (3) or as an inhibitor in the solution (2) unless chloride ion is present in the solution. This study has shown that, unless chloride ion is present in solution, molybdenum becomes depleted in anodic films during repassivation. A previous study (3) also showed that repassivation kinetics in chloride containing solutions were proportional to the concentration of molybdenum in the alloy. A final observation from previous studies (2, 3) was that a condition of restricted solution mass transport was required for molybdenum additions to become effective. The role of the restricted mass transport condition is not only to create a situation requiring a minimum value of concentration of $MoO_4^=$, but also a minimum value of Cl^- ion to synergistically interact with the inhibitor ion.

The fact that higher molybdenum containing alloys, which repassivated more rapidly, were found to contain higher amounts of chlorine in the anodic film further points to a synergistic interaction between the two species. It is difficult to explain the increased repassivation kinetics Fe-5Mo over Fe-1Mo on the basis of an insoluble molybdate salt film since XPS results do not show any enrichment of Mo, even under restricted mass transport conditions, for anodic films grown without chloride ion. In the presence of chloride ion, however, anodic films are enriched in molybdenum, as well as in chlorine, at least with respect to films grown without chlorides in solution.

Therefore, although the formation of a molybdate salt film is not reasonable, the existance of a chloride salt film is. The properties of such a chloride salt film should become important in controlling repassivation kinetics and in overall resistance to localized corrosion attack. The role of molybdenum appears to be in stabilizing a chloride salt film rather than in affecting repassivation of the substrate directly. Sakashita and Sato (4) have recently suggested that molybdate ion, by adsorption on a surface film, can alter transport properties of that film. The formation of a chloride salt film is suggested by the results shown in figure 5 in which chloride ion concentration at the surface is proportional to molybdenum concentration in the alloy.

Other recently published results on the effect of molybdenum additions to ferric stainless steels (5) have also demonstrated that chloride ion (as well as alloyed chromium) is required for the beneficial effect of the molybdenum to be exhibited.

On the basis of these results then, it can be concluded that although there is a definite increase in the rate of repassivation of iron in chloride containing solutions as a result of molybdenum addition, this beneficial contribution is not due to the formation of a molybdate salt film, but rather is due to the stabilization, by molybdate ion, of a chloride salt film. In all probability, however, once the repassivation transient is over, the chloride film will eventually hydrolyze to an oxide film. This film can also be stabilized by molybdate ion adsorption, as has been suggested by Sakashita and Sato (4). This last statement is also consistent with what has been observed regarding the inhibition of pit propagation on iron in chloride solutions by molybdate ion (2), in which molybdenum, but little chloride ion, was found within the repassivated pits.

Conclusions

1. Molybdenum is depleted in surface films on iron-molybdenum binary alloys.

2. Concentration of molybdenum in surface films is measureably increased when films are grown in the presence of chloride ion.

3. Effective repassivation of iron-molybdenum binaries requires some kind of synergistic interplay between the molybdate and chloride ions.

4. It is suggested that $MoO_4^{=}$ acts as an inhibitor in two stages:

   a) State I - Synergistic interaction with Cl^- ion to stabilize a Cl^- salt film.

   b) Stage II - Synergistic interaction with an iron oxide to stabilize a passive film.

References

1. J. B. Lumsden and R. W. Staehle, Scr. Met., Vol. 6, p. 1205 (1972).

2. Office of Naval Research, NAONR 18-69, "The Role of Passive Film Growth Kinetics and Properties in Stress Corrosion Susceptibility", NBSIR 75-916, October 1975.

3. Ibid., NBSIR 76-1170, November 1976.

4. M. Sakashita and N. Sato, Corrosion Science, 17, No. 6, 473 (1977).

5. K. Sugimoto and Y. Sanada, Corrosion Science, 17, No. 6, 473 (1977).

Figure Captions

Figure 1 XPS spectrogram of air-formed film on pure molybdenum. Plotted are counts (2-10K) versus energy and shown are the Mo 3d peaks.

Figure 2 Plots of peak height ratio data from Table 1. Shown are Mo/Fe for 4 surface conditions of both Fe-1Mo and Fe-5Mo alloys as well as $Mo_{(m)}/M_{(ox)}$ and $Fe_{(m)}/Fe_{(ox)}$ ratios.

Figure 3 XPS spectra for surface films following anodic passivation at 442 mV SHE without chloride ion; (solid line). This spectrum is compared to the spectrum obtained for the air-formed film (dashed line) on Fe-5Mo. Kinetic energy increases along abscissa.

Figure 4 XPS spectrogram for surface film following anodic passivation at 442 mV SHE with chloride ion (short dash line); this spectrum is overlaid on the spectrum obtained for the air-formed film on Fe-5Mo (long dash line) for comparison.

Figure 5 Comparison of XPS spectra for Fe-1Mo (solid line) and Fe-5Mo (dashed line) in chloride solutions after anodic passivation at 442 mV SHE.

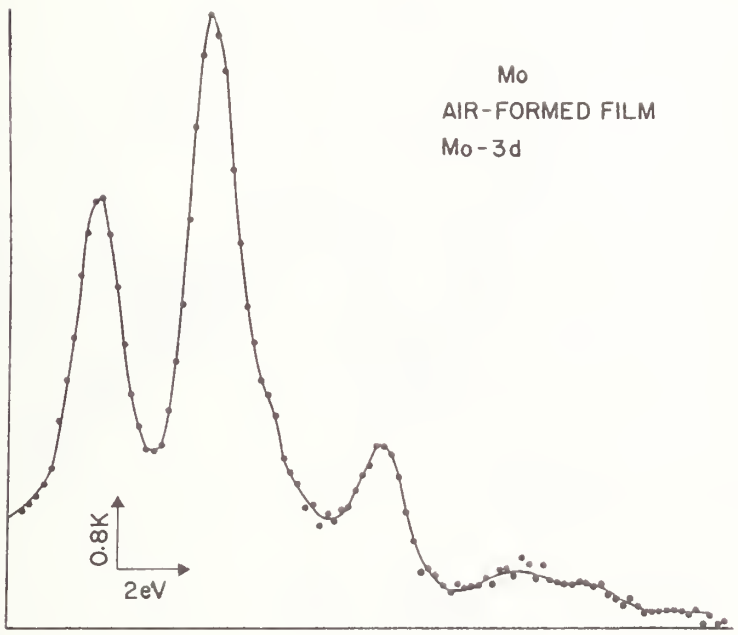

Figure 1

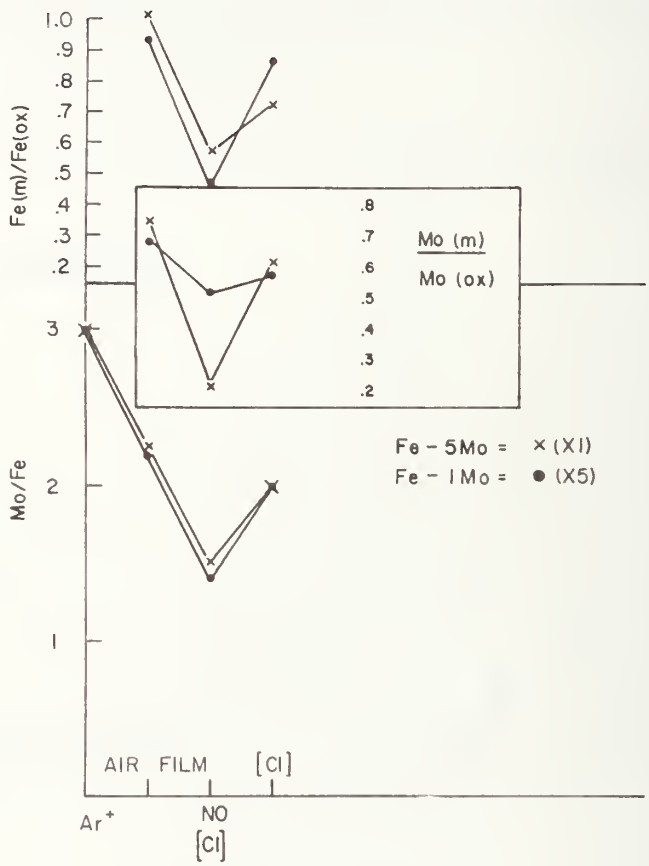
1.0
.9
.8
.7
.6
.5
.4
.3
.2
Fe(m)/Fe(ox)
3
2
1
Mo/Fe
.8
.7
.6
.5
.4
.3
.2
Mo (m)
Mo (ox)
Fe - 5Mo = × (X1)
Fe - 1Mo = ● (X5)
AIR
FILM
[Cl]
Ar+
NO
[Cl]

Figure 2

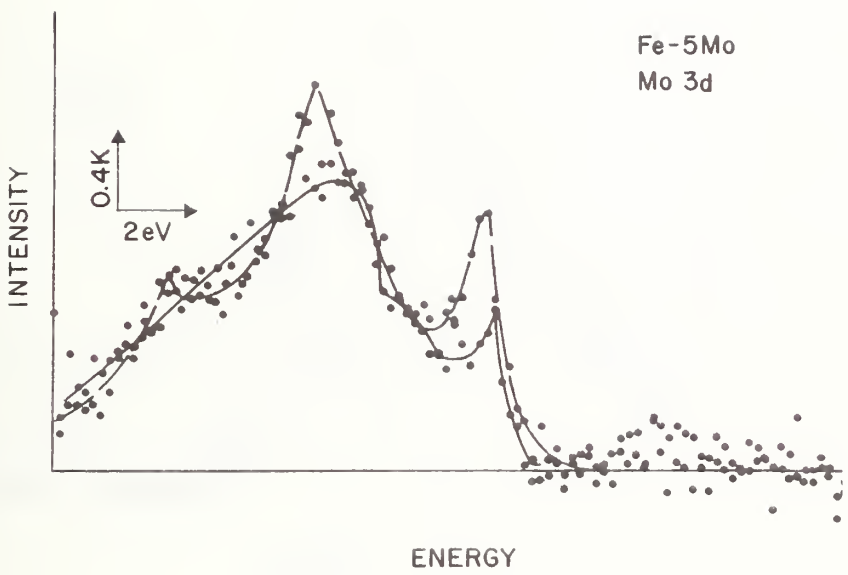

Figure 3

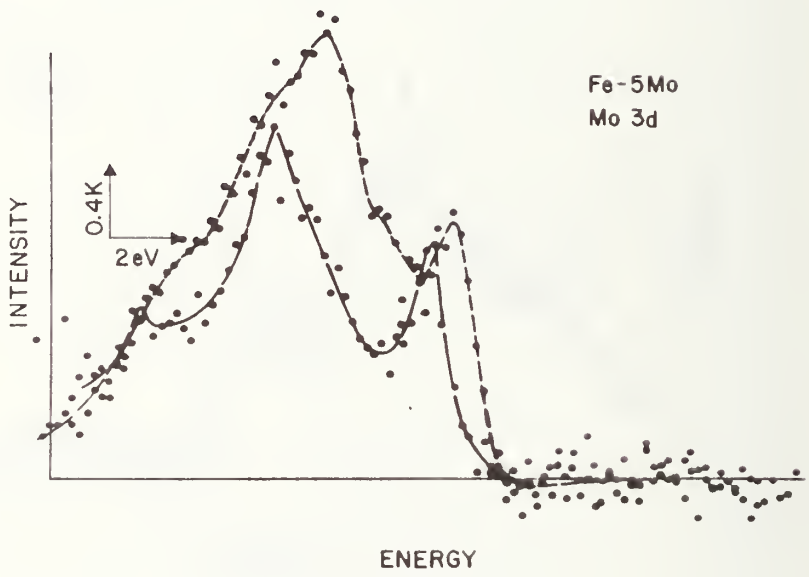

Figure 4

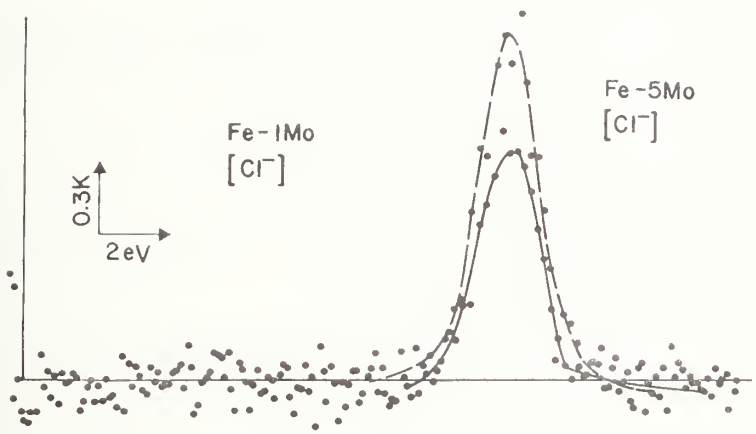

Figure 5

NBS-114A (REV. 11-77)

U.S. DEPT. OF COMM. BIBLIOGRAPHIC DATA SHEET	1. PUBLICATION OR REPORT NO. NBSIR 78-1429	2. Gov't Accession No.	3. Recipient's Accession No.

4. TITLE AND SUBTITLE

The Role of Passive Film Growth Kinetics and Properties in Stress Corrosion and Crevice Corrosion Susceptibility

5. Publication Date MAY 1978

6. Performing Organization Code

7. AUTHOR(S)

J. Kruger, J. R. Ambrose, J. J. Carroll, and A. J. Melmed

8. Performing Organ. Report No.

9. PERFORMING ORGANIZATION NAME AND ADDRESS

NATIONAL BUREAU OF STANDARDS
DEPARTMENT OF COMMERCE
WASHINGTON, D.C. 20234

10. Project/Task/Work Unit No. 3120448

11. Contract/Grant No. NAONR 18-69, NR036-082

12. Sponsoring Organization Name and Complete Address (Street, City, State, ZIP)

Office of Naval Research
Department of the Navy
Arlington, VA 22217

13. Type of Report & Period Covered interim 12/76-12/77

14. Sponsoring Agency Code

15. SUPPLEMENTARY NOTES

16. ABSTRACT *(A 200-word or less factual summary of most significant information. If document includes a significant bibliography or literature survey, mention it here.)*

This report consists of the following four parts:

I - Field Ion Microscopy Studies of the Interaction of Hydrogen with Selected Metals and Alloys

II - The Role of Noncrystalline Films in Passivation and Breakdown of Passivation

III - Effect of Chromium Depletion on the Repassivation Kinetics 18-10 Austenitic Stainless Steel in Sodium Chloride Solutions

IV - Composition of Surface Films Formed During the Repassivation of Iron and Iron-Molybdenum Alloys

17. KEY WORDS *(six to twelve entries; alphabetical order; capitalize only the first letter of the first key word unless a proper name; separated by semicolons)* Crevice corrosion; field ion microscopy; iron; noncrystalline films; passive films; repassivation; sensitization; stainless steel; uranium; x-ray photoelectron spectroscopy

18. AVAILABILITY

[X] Unlimited

[ ] For Official Distribution. Do Not Release to NTIS

[ ] Order From Sup. of Doc., U.S. Government Printing Office Washington, D.C. 20402, SD Stock No. SN003-003

[X] Order From National Technical Information Service (NTIS) Springfield, Virginia 22151

19. SECURITY CLASS (THIS REPORT)	21. NO. OF PAGES
UNCLASSIFIED	67
20. SECURITY CLASS (THIS PAGE)	**22. Price**
UNCLASSIFIED	$5.25

USCOMM-DC 66035-P78

78-1430

nstrument to Evaluate alled Smoke Detectors

. Lee

ire Research
Applied Technology
eau of Standards
, D.C. 20234

February 1978

Final Report

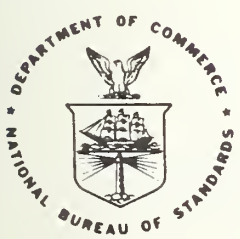

U.S. DEPARTMENT OF COMMERCE

NATIONAL BUREAU OF STANDARDS